NON-FERMI LIQUID GROUND STATES
IN
CERTAIN HEAVY FERMIONS

A thesis submitted to the

Division of Research and Advanced Studies
of the University of Cincinnati

in partial fulfillment of the
requirements for the degree of

DOCTOR OF PHILOSOPHY

in the Department of Physics
of the College of Arts and Sciences

1998

by

Amit Chattopadhyay

B.Sc., Indian Institute of Technology, Kharagpur, 1987
M.Sc., Indian Institute of Technology, Kharagpur, 1989
M.S., Indiana University, 1991

Committee Chair: Mark Jarrell

Acknowledgments

I would like to thank Mark Jarrell for all the guidance he provided throughout my time here in Cincinnati. Without his help in suggesting problems and strategies, little or none of this work would have been possible. I thank him for providing the opportunity to visit collaborators, for being patient while I dabbled with different problems, and for the numerous nice dinners at his place.

Special thanks go to Bill Joiner and Brian Meadows for agreeing to join this thesis committee.

I am grateful to H. R. Krishnamurthy and Michael Ma, whose advice and comments have been greatly beneficial. Their physical intuition and sharp counter-arguments are resources I was lucky to draw on; hopefully it has made me intellectually somewhat honest. The more open-ended arguments with Michael about His Airness Michael were pleasurable, to say the least.

Without Laurie and Moitreyee, it would have been difficult to recall pleasant memories of graduate school. I shall very fondly remember the time that I have spent with them; it is far more valuable to me than this thesis. Aditi, Anuvrat, Saroj, Niki, Alex, Bob, Ricardo, Raja and many others provided their individual perspectives on physics, life and essentially everything else.

I would like to sincerely thank the members of the physics department office for all the help they provided. Lynne, Donna and Peg clinically smoothed out the administrative edges numerous times.

Finally, I owe an overwhelming amount of gratitude to my parents and my brother. They have been unconditionally patient and supportive throughout my prolonged education.

Contents

1 Introduction **6**

2 Fermi-liquid theory, Kondo effect and the Anderson Hamiltonian **8**

2.1 Fermi-liquid theory 8

2.1.1 Observable properties of a Fermi-liquid 9

2.2 Kondo effect and the Anderson Hamiltonian 12

2.2.1 Kondo model 15

2.2.2 Anderson Hamiltonian 16

2.2.3 Unitarity limit 17

3 Overview of the relevant experiments; thermodynamic and transport measurements **19**

3.1 Non fermi-liquid heavy fermions 19

3.2 Proposed scenarios 20

4 Models and Methods of Solution **27**

4.1 Limit of Infinite Spatial Dimensions 27

4.2 Dynamical Mean Field Approximation 30

4.2.1 DMF for a dilute system 33

4.3 The Method of Quantum Monte Carlo 34

4.3.1 QMC updating 35

4.4 Maximum Entropy method 38

5 Non Fermi liquid dynamics of disordered heavy fermions 43

5.1 Introduction. 43

5.2 Formalism. 45

5.3 Results 48

5.4 Conclusion. 56

6 Weak magnetoresistance of disordered heavy fermion systems 58

6.1 Introduction 58

6.2 Formalism 59

6.2.1 Extension of the Doniach-Sunjic form 59

6.3 Results 61

6.4 Conclusion 70

7 Non Fermi Liquid Dynamics of the Two-Channel Kondo Lattice 71

7.1 Introduction 71

7.2 Motivation and Model 72

7.3 Formalism and Simulation 74

7.4 Results 75

List of Figures

2.1 Scattering in a Fermi liquid 10

2.2 Fermi-liquid response functions 13

2.3 Kondo physics in $La_1 - xCe_xB_6$ 14

3.1 Log divergence in specific heat data 21

3.2 Log divergence in specific heat data 22

3.3 Resistivity data for $Y_{1-x}U_xPd_3$ at various x 23

3.4 Linear resistivity in $Y_{0.8}U_{0.2}Pd_3$ 24

3.5 Optical conductivity of $UCu_{3.5}Pd_{1.5}$ 26

3.6 Optical scattering rate in $UCu_{3.5}Pd_{1.5}$ 26

4.1 second order contribution to the self energy of the Hubbard model . . 29

4.2 dynamical mean field algorithm 31

4.3 first few diagrams for the self energy of the Hubbard model 32

5.1 Spectral function for Anderson impurity at T≠0 47

5.2 Kondo disorder averaged self-energy 50

5.3 Relevant distribution of Kondo scales 51

5.4 Calculated optical conductivity within Kondo disorder model 53

5.5 Calculated $\Gamma(\omega)$ and $m^{*}(\omega)$ for Kondo disorder 55

6.1 Up-spin Anderson impurity spectrum at finite field 62

6.2 Theoretical and experimental magneto-resistance 64

6.3 Susceptibility curves for different Kondo scales 65

6.4 Resistivity curves for different Kondo scales 66

6.5 Role of H and T within the $P(T_K)$ scenario 67

6.6 Differential field effects on transport and thermodynamics 69

7.1 Scaling trajectory of the two channel impurity 72

7.2 Self-energy and density of states of the 2-channel lattice 77

7.3 Linear resistivity of the 2-channel lattice 79

7.4 Optical conductivity of the 2-channel lattice 81

7.5 Optical scattering rate and effective mass 82

Chapter 1

Introduction

For the past four decades, Landau's phenomenological theory of an interacting Fermi system has served as a paradigm for our understanding of metallic behaviour. However, some recent experiments on Ce and U compounds have opened up the possibility of a metallic state which is not a Fermi-liquid. Our objective in this thesis is to try and understand this breakdown of Fermi-liquid theory, and we start with a brief review of Landau's theory in Chap. 2. We begin with the notion of a "quasiparticle" and state how the low-energy transport and thermodynamic response functions depend on the effective mass m^* of the quasiparticles. We also discuss a slightly different incarnation of the Fermi-liquid that shows up at low temperatures in the Kondo and Anderson models, of magnetic impurities in metals. Here the low-energy excitations can be parametrized with the effective mass as well, which is now related to the inverse of the Kondo temperature T_K.

In Chap. 3 we present an overview of the experimental scenario, mostly in Ce and U intermetallics which definitely exhibit Kondo-esque logarithmic scattering behaviour at high temperatures. The ground state in these compounds is a paramagnetic metal with a high residual resistivity, but they seem to violate the canonical Fermi-liquid description. We concentrate on two possible mechanisms that can give rise to these anomalous metallic states, namely disorder and Kondo over-screening. The effect of disorder is to create rare regions in the system with a Kondo scale that is essentially zero, thereby destroying the Fermi-liquid. Chap. 4 outlines the methods of solution of correlated impurity and lattice problems; dynamical mean-field theory maps the lattice onto a self-consistently determined Anderson impurity, then Quantum Monte Carlo solves the impurity problem. Using these techniques, the consequences of Kondo disorder in dynamics and magneto-transport are calculated in Chaps. 5 and 6 respectively. Kondo overscreening results from the inability of the conducting host to screen out the magnetic impurity at the largest length scales, or equivalently, the smallest temperatures. Dynamics of an over-screened Kondo lattice is studied in Chap. 7.

Chapter 2

Fermi-liquid theory, Kondo effect and the Anderson Hamiltonian

2.1 Fermi-liquid theory

Landau's idea is to start from a completely non-interacting Fermi gas and adiabatically turn on the interactions between the particles. There will be a one-to-one correspondence between states before and and after this adiabatic turning-on process, so that the new states can be labeled with the quantum numbers of the old and they will be in roughly the same order in energy. The noninteracting gas can be described as having a distribution function $n(k)$ (assumed to be very close to the $T = 0$ Fermi distribution of the ground state), so the new states can be labeled by $n(k)$ as well. The fictional particles that occupy the states k are called "quasiparticles".

It is important to note that the interactions are turned on, not infinitely slowly, but at a slow rate R chosen with two conditions in mind [1] :

1) If we are considering states of excitation of the system which correspond roughly to temperature T, i.e. excitations (holes below or particles above the Fermi sea) having energies $\sim T$, $R << T$ will ensure an appropriate energy resolution.

2) If τ is the lifetime of the quasiparticles, we must have $R >> \frac{1}{\tau}$. Hence for low enough T, we have $T >> \frac{1}{\tau}$ which is an essential condition for the success of Fermi-liquid theory. The quasiparticles have infinite lifetime at, and are well defined only in the vicinity of the Fermi energy.

A signature of an interacting Fermi system is the presence of a finite quasiparticle weight Z, that shows up as a discontinuity in the bare-particle distribution function $n(k)$ at the Fermi surface (Fig. 2.2). Z can be understood as the fraction of the bare particle contained in the quasiparticle, and hence is bounded between 0 and 1. When k crosses k_F (the Fermi momentum), the excitations change from quasiparticle to quasi-hole. The notion of a quasiparicle can be used to calculate low-energy observables in this theory, as done in the next section.

2.1.1 Observable properties of a Fermi-liquid

Among the numerous measurable properties, we are going to restrict ourselves to a brief discussion of the resistivity and mention how it, along with the magnetic susceptibility and specific heat, depends on the single relevant scale in the theory, the Fermi momentum k_F.

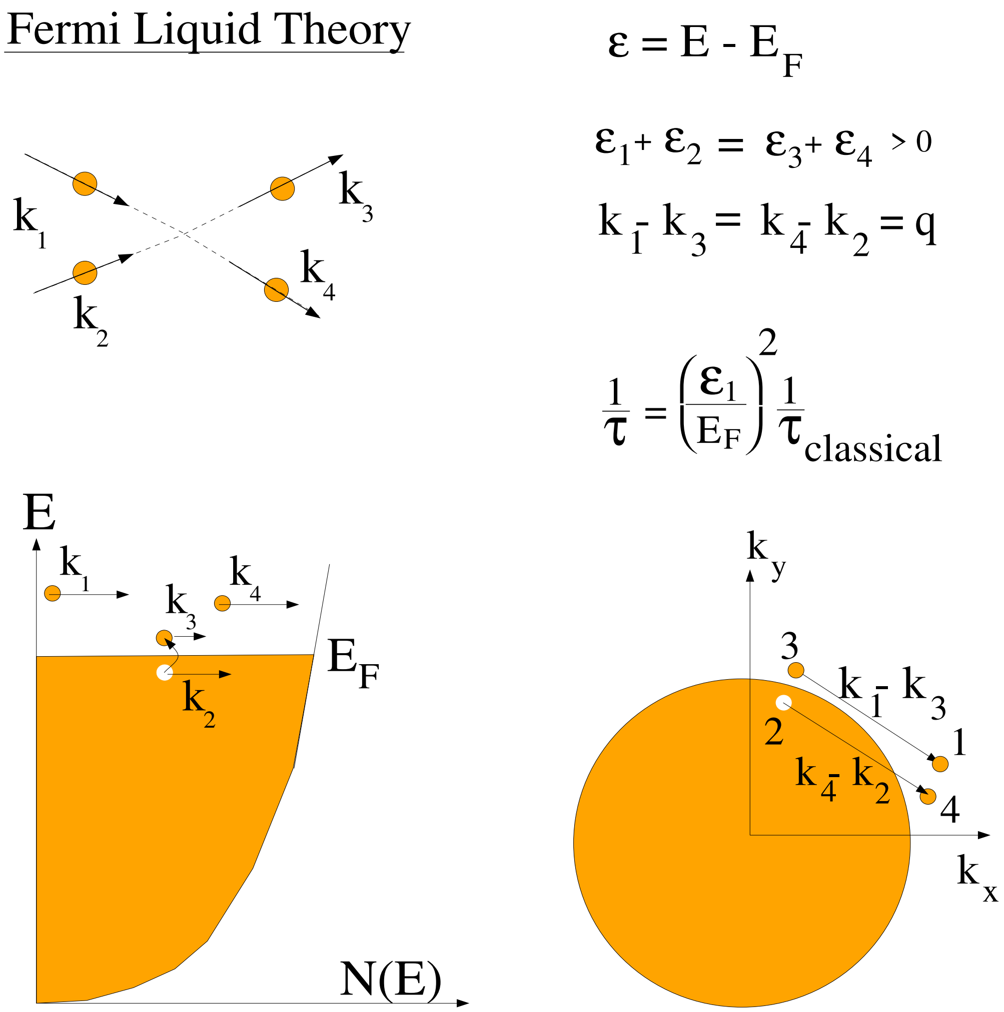

Figure 2.1: *The simplest decay process that can happen to a particle with a momentum* $\mathbf{k_1}$. *The scattering rate* $\frac{1}{\tau}$ *can be estimated using Golden Rule and phase space restrictions.*

The simplest decay process that can happen to a particle **1** is to excite **2** out of the Fermi sea, into an empty state **4** and itself get scattered into the state **3** (Fig. 2.1). With $\mathbf{q}$ being the momentum transfer as defined in the figure, let us call the scattering potential $V(\mathbf{q})$.

To do a perturbative calculation for the decay rate, we need the energy change in this process which is

$$\Omega = \epsilon_3 + \epsilon_4 - \epsilon_1 - \epsilon_2 \tag{2.1}$$

with all energies measured from the Fermi energy. The decay rate would then be given by

$$\begin{aligned} \frac{1}{\tau} &= \lim_{\eta \to 0} \int d^3q \, d^3k_2 \, |V(\mathbf{q})|^2 \, Im \left(\frac{1}{\Omega - \imath\eta} \right) \\ &= \pi \int d^3q \, d^3k_2 \delta(\Omega) \, |V(\mathbf{q})|^2 \end{aligned} \tag{2.2}$$

which is Fermi's golden rule. Momentum conservation is reflected in the fact that we have only two $\mathbf{k}$ integrals.

For the δ function to give a finite result, all three of the excitation energies ϵ_3, ϵ_4 and $-\epsilon_2$, must be less than ϵ_1. This means that, in Eq. 2.2, both the integrals are restricted to an amount $\sim \epsilon_1$ of the available energy space. Using this phase space restriction it can be shown that the scattering rate of a particle of energy ϵ_1 is

$$\frac{1}{\tau(\epsilon_1)} = const. \left(\frac{\epsilon_1}{E_F} \right)^2 . \tag{2.3}$$

In calculating the resistivity, the energy ϵ_1 is averaged over a region near the Fermi surface of width $k_B T$. This gives rise to

$$\rho(T) = const. \left(\frac{T}{E_F}\right)^2 . \tag{2.4}$$

A fundamental parameter of the theory is the effective mass m^*, which can be defined in terms of the density of states or group velocity at the Fermi surface $N(E_F)$

$$\begin{aligned} \frac{k_F}{m^*} &= \frac{d\epsilon_k}{dk}\,|_{k_F} \\ \Rightarrow m^* &= \frac{\pi^2 N(E_F)}{k_F}. \end{aligned} \tag{2.5}$$

Starting with m^*, one can find the specific heat coefficient $\gamma = C_V/T$ and the magnetic susceptibility χ for the Fermi liquid to be (to lowest order in T)

$$\gamma = \frac{m^* k_F k_B^2}{3}; \qquad \chi = \frac{m^* k_F}{4\pi^2(1+Z_0)} \tag{2.6}$$

where Z_0 is a Landau parameter, that measures the "polarizability" of the system [2]. The salient features of a Fermi-liquid are summarized in Fig. 2.2.

2.2 Kondo effect and the Anderson Hamiltonian

In general, when an impurity atom is introduced into a metal, the conduction electron states are disturbed by the local potential change induced by the impurity. The electronic states of the impurity atom also change at the same time; such a change of states should show up also in the magnetism of these materials. The original Kondo

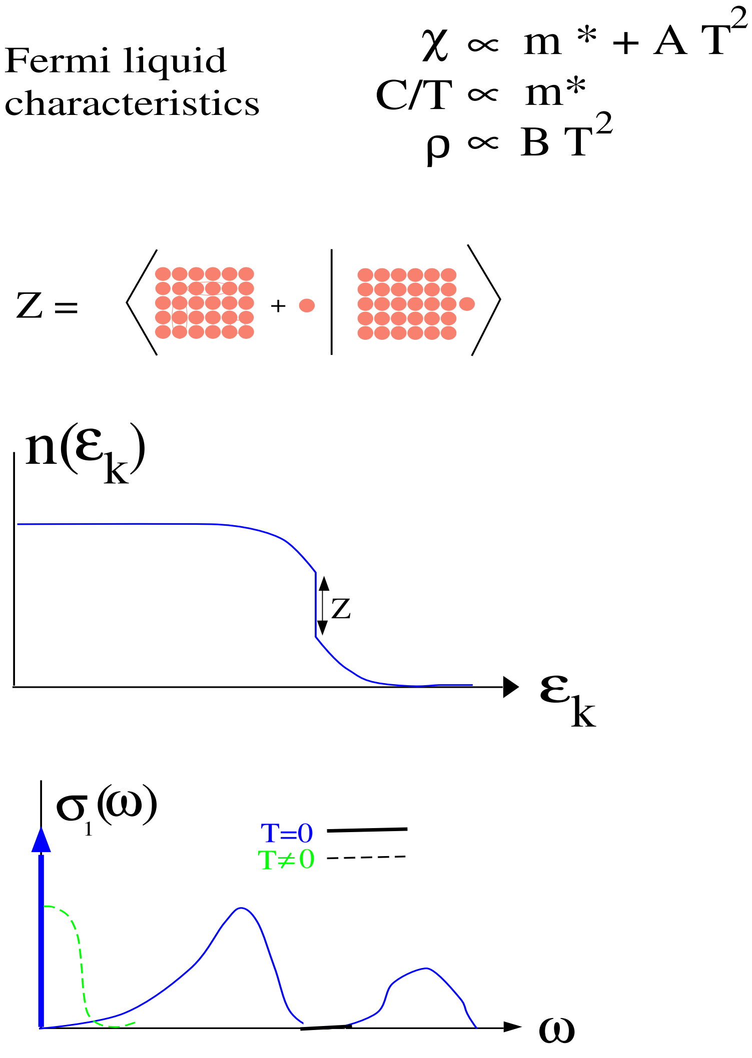

Figure 2.2: *The thermodynamic and transport relations of a Fermi liquid are shown here. The interaction is reflected through a finite quasiparticle width Z in the distribution $n(\epsilon_k)$; the translation invariance of the system gives a δ-function peak in the optical conductivity $\sigma_1(\omega)$. It smears out by $O(T^2)$ at finite T.*

problem was introduced to describe a single additional magnetic impurity with a free spin, embedded in a metal and interacting with the metal electrons via a exchange scattering potential. This rather specialized and unphysical problem seems to contain the essential difficulties of a fairly wide class of magnetic impurities in metals. Characteristic "Kondo behaviour" in a metal includes rather large scattering effects at moderate temperatures, anomalous temperature dependence of the resistance and at low T, a tendency to exhibit non-magnetic but very strongly scattering behaviour (Fig. 2.3) [6].

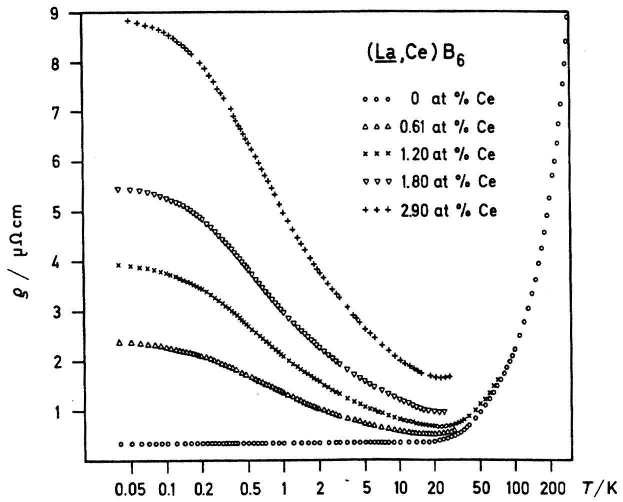

Figure 2.3: *Electrical resistivity of* LaB_6 *and four* $La_1 - xCe_xB_6$ *samples as a function of temperature.* $\rho(T = 0)$ *normalized for each impurity is nailed at the unitarity limit, where the scattering phase shifts are* $\frac{\pi}{2}$ *at the Fermi level. In this particular case,* $\rho_{unitary}$ *can be estimated to be* $\sim 2.77\mu\Omega cm$ *(the unitarity limit is discussed in the last section of this chapter).*

2.2.1 Kondo model

The Kondo model consists of a single spin degree of freedom coupled to the conduction electrons of a metallic host via an antiferromagnetic exchange interaction as seen in the following Hamiltonian;

$$H = \sum_{\mathbf{k},\sigma} \epsilon_{\mathbf{k}} n_{\mathbf{k},\sigma} - J\mathbf{S}.\mathbf{s}(0) \quad . \tag{2.7}$$

$n_{\mathbf{k},\sigma} = d^{\dagger}_{\mathbf{k},\sigma} d_{\mathbf{k},\sigma}$ is the number operator of conduction electrons with spin σ and momentum $\mathbf{k}$, $J < 0$ is the antiferromagnetic exchange, $\mathbf{S}$ is the impurity spin and $\mathbf{s}(0)$ is the conduction electron spin-density at the position of impurity. Perturbative calculations in J can explain the logarithmic upturn in the resistivity observed in dilute magnetic alloys (Fig. 3). They also hint towards the existence of a natural energy scale T_K for this problem called the "Kondo temperature". Non-perturbative renormalization group (RG) approaches can account for the existence of this natural energy scale and its consequences. Anderson's "Poor Man's scaling" located the fixed points in this problem, indicating that the effective antiferromagnetic exchange J is actually a "running" constant and scales with T such that it rapidly increases in magnitude when T is lowered below T_K and eventually diverges as $T \rightarrow 0$. Wilson's combined numerical and analytical RG approach established that the temperature dependent effective moment, $\mu^2_{eff}(T) = 3T\chi(T)$, vanishes for $T \rightarrow 0$, and that the moment obeys a simple scaling relation $\mu^2_{eff}(T) = F(T/T_K)$, with F being a universal function[3].

2.2.2 Anderson Hamiltonian

One good way of thinking about the Kondo model (Eq. 2.7) is that it is an effective Hamiltonian for low-energy processes, which follows from the symmetric version of the Anderson Hamiltonian [4]

$$
\begin{aligned}
H &= \sum_{\mathbf{k},\sigma} (\epsilon_{\mathbf{k}} + \epsilon_d)\, n_{\mathbf{k},\sigma} \\
&+ \sum_{\sigma} \epsilon_f n_{f,\sigma} + U(n_{f,\uparrow} - 1/2)(n_{f,\downarrow} - 1/2) \\
&+ V \sum_{\mathbf{k},\sigma} \left(d^{\dagger}_{\mathbf{k},\sigma} f_{\sigma} + \mathrm{H.c.} \right) \quad . \qquad (2.8)
\end{aligned}
$$

Eq. 2.8 consists of three parts which describe the conduction (d) electrons , the impurity (f) electrons and a hybridization between the two (denoted by V). Here the creation operators are denoted by $d^{\dagger}_{\mathbf{k},\sigma}$ for conduction electrons and f_{σ} for the impurity electron with the corresponding number operators $n_{\mathbf{k},\sigma}$ and $n_{f,\sigma}$. ϵ_d and ϵ_f are the bare energy levels of the d and f electrons respectively. $U > 0$ is a strong Coulomb correlation between the localized f-electrons and penalizes the double occupancy of a local orbital. The symmetric version of the Anderson model is obtained by setting the energy of the doubly occupied f-state ($2\epsilon_f + U$) to be equal to that of the unoccupied f-state (0) in the Anderson Hamiltonian . Making U very large would now eliminate both of these states (energy $\sim \frac{U}{2}$) from the Hilbert space, leaving us with a single f-spin interacting with a conduction electron bath (Eq. 2.7). The Kondo model can be formally derived from Eq. 2.8 by a canonical transformation in the limit $\epsilon_f \to -\infty$, $V \to \infty$, $U \to \infty$ and $8V^2/U = J$[5].

The antiferromagnetic interaction J, taking advantage of the constant density of states ϵ_k down to $\epsilon_k = 0$, can form a bound state between the local spin and one made from the free-electron states. Writing a variational wave function, one estimates the binding energy of this state to be of order

$$k_B T_K = D e^{-\frac{1}{J\rho}} \tag{2.9}$$

where D is the bandwidth ($\sim \frac{U}{2}$) and ρ the density of states. This is the ground state of the Kondo model, which is a nonmagnetic singlet due to the compensation of the impurity spin by the conduction electron "cloud". This low energy scale suggests a correspondingly large length scale $\xi_K = \frac{\hbar v_F}{T_K}$, which can be thought of as the "size" of the Kondo screening cloud. Noziéres' showed that the ground state of the Kondo model is a Fermi-liquid, with an effective Fermi energy T_K. Analogous to their behaviour for a generic metal at low T, the susceptibility $\chi(T)$ and specific heat coefficient $\gamma(T)$ for the Kondo system are constant and proportional to $\frac{1}{T_K}$ at $T << T_K$ (they are related to each other through the Wilson ratio). On the other hand, when $T > T_K$ there is a free spin undergoing spin-flip scattering, and its magnetic properties include a Curie susceptibility.

2.2.3 Unitarity limit

In the Kondo or Anderson model, the scattering centre has an internal degree of freedom, its spin direction, unlike an ordinary nonmagnetic scatterer. This degree of freedom is reflected in a large peak at or near E_F in the conduction-electron scattering rate as a function of energy. As $T \to 0$, only electrons with energy near E_F carry current, and these electrons are strongly scattered by the local moment. Because the Anderson Hamiltonian has its origin in a resonant interaction between the conduction electrons and the f-orbitals (for Ce or U) on the local moment, only the relevant ($l = 3$ or f) partial wave of the incoming conduction electron is scattered strongly.

As T decreases below T_K, the divergence in $\rho(T)$ must saturate when all of the f-wave is being scattered, and the resistivity cannot increase above the value [6]

$$\rho_{unitary} = (2l+1)\frac{2m^* x}{\pi \hbar z e^2 N(E_F)} \tag{2.10}$$

where $l = 3$ for f-wave (m^* = effective mass, x= concentration of impurities, z= number of conduction electrons per host atom) . It is basically $(2l+1)$ times the unitarity limit for s-wave ($l = 0$) scattering and corresponds to the scattering phase shift being $\frac{\pi}{2}$ at the Fermi level at $T = 0$. This equation represents the limit imposed on the total amount of l-wave scattering by the unitarity of the S-matrix, and a detailed derivation can be found in [7].

Chapter 3

Overview of the relevant experiments; thermodynamic and transport measurements

3.1 Non fermi-liquid heavy fermions

Fermi-liquid theory, briefly outlined in the previous chapter, has become the canonical description of concentrated Kondo or heavy fermion systems, principally alloys and intermetallic compounds of lanthanide (Ce,Yb) and actinide (U) ions. Conventional heavy fermion f-electron compounds, such as $CeAl_3$ and UPt_3 behave as Fermi liquids, in spite of the strong electron-electron interactions that renormalize the effective mass of the electron m^* by a factor of $\sim 10^2 - 10^3$! Equivalently, there is a low "effective" Fermi temperature $\sim 1 - 10K$ and this sets the coherent scale of the system at low T.

However, a large and growing number of heavy-fermion metallic alloys do not exhibit this Fermi-liquid behaviour. Thermal and transport properties of these non-Fermi-liquid (NFL) materials as $T \to 0$ seem to fall into a limited number of classes;

most(not all) exhibit a logarithmic divergence of $\gamma(T)$ as shown in Fig. 3.2 [8] and a linear departure of $\rho(T)$ from its value at $T = 0$ (Fig. 3.3, 3.4)[8]. The susceptibility is reported to vary either as $1 - b(T/T_K)^{1/2}$ or as $\ln(bT/T_K)$, where T_K is the Kondo temperature and b is a dimensionless factor of order unity. Both Ce- and U-based alloys exhibit NFL behaviour, but we are going to limit our discussion to the Uranium compounds. This is for reasons of simplicity: in Ce-intermetallics like $CeCu_{5.9}Au_{0.1}$ where one observes the NFL features, there is quite often a low temperature spin-glass or other magnetic transition [11]. A very simplistic reason could be that the impurity-conduction coupling J in Ce-systems is such that T_{RKKY} ($\sim J^2/D$) competes strongly with T_K ($\sim De^{-\frac{D}{J}}$), hence the spin-glass ordering (Fig. 3.1). The parameter space of U-based alloys provide a paramagnetic region that is clearly Kondo-dominated [9], which is where we concentrate. We would like to state that the competition between the Kondo and RKKY scales in real materials would involve the inter-impurity distances as well, and requires a far more careful analysis. As an example, the inter-f distance in UBe_{13} is known to be more than that in $CeBe_{13}$, thereby enhancing RKKY in the Ce-system. However, in disordered systems the situation is more complicated.

3.2 Proposed scenarios

A number of mechanisms have been proposed to acount for the breakbown of a Fermi-liquid ground state. The leading candidates include

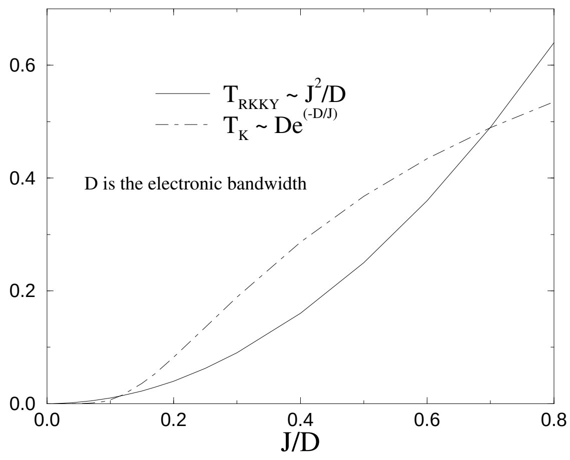

Figure 3.1: *The Kondo and RKKY energy scales as a function of the impurity-conduction band coupling J. For U-intermetallics, the values of J are in the region where T_K dominates over T_{RKKY}. At very low values of J, there can be spin-glass ordering because of dominant RKKY. This could be happening in the Ce-compounds.*

- An inhomogeneous distribution of Kondo temperatures due to structural disorder in the alloy, referred to as 'Kondo disorder'. [14]

- The multichannel Kondo impurity where the ground state is an overscreened moment, and its lattice version.[13]

- Proximity to a zero-temperature quantum critical point.[12]

In this thesis, I shall be concerned with systems where the breakdown of the Fermi-liquid at low temperatures is believed to be due to either of the first two reasons. For the Kondo disorder, we compare our calculations (qualitatively) with

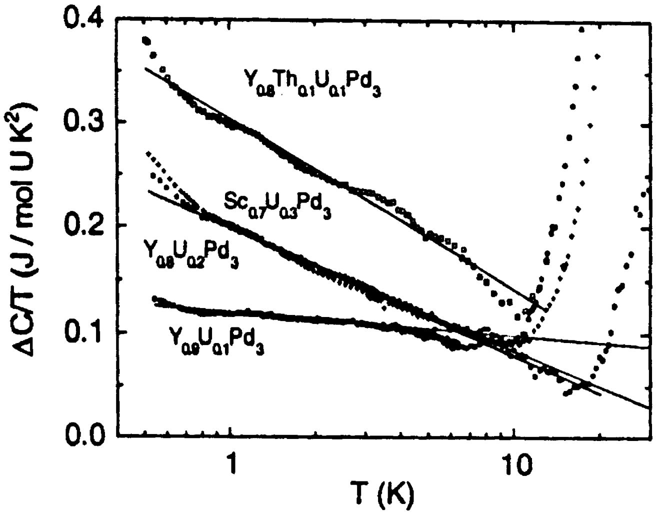

Figure 3.2: *Low temperature specific heat $\Delta C/T$ versus $\log T$ for various Kondo alloys which exhibit a $T = 0$ logarithmic divergence, a non Fermi liquid behaviour. Solid lines are fits of the data to the form $\Delta C/T = -(0.251/T_K)R\ln(T/0.41T_K) + B'$, where B' is a constant.*

data on $UCu_{5-x}Pd_x$ and $Y_{0.8}U_{0.2}Pd_3$ which are heavy fermion systems with clear signatures of disorder. The multichannel Kondo lattice model seems to have quite a bit of mystique attached to it, and UBe_{13} is one candidate with probably the least ambiguity. We don't display the experimental results from this compound, but point to the appropriate references in Chap. 7.

It is rather remarkable that transport and thermodynamic measurements on $UCu_{5-x}Pd_x$ [8, 15] which has an ordered f-sublattice with distorted ligands, are qualitatively so similar to those on a "dilute" system like $Y_{0.8}U_{0.2}Pd_3$ [9, 16], where the disorder is a substitutional Uranium impurity. In Fig. 3.3 one notices the impurity-like large incoherent scattering for x=0.2. For higher x, the f-electrons start forming a lattice of their own and the resistivity drops due to the onset of coherence [9]. A very similar sequence of features is observed in the other set of compounds with an increase in Pd concentration. From now on we will address these systems under the implicit assumption that they are equivalent.

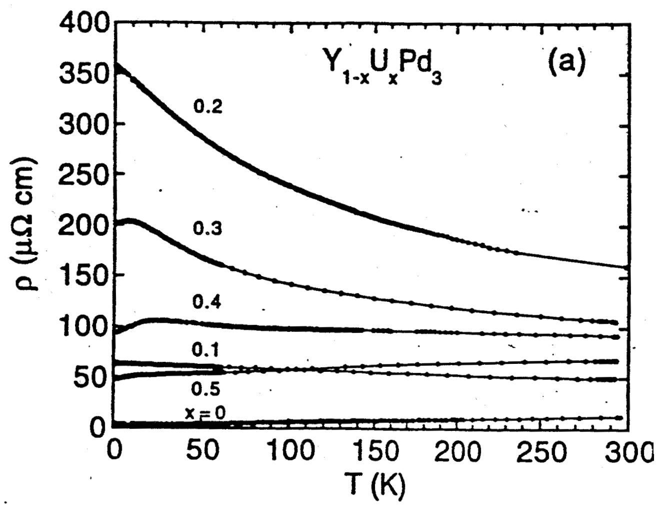

Figure 3.3: *Electrical resistivity* ρ *against* T *of* $Y_{1-x}U_xPd_3$ *for various values of* x *in the range* $0 \leq x \leq 0.5$. *Important:* $\rho(T)$ *shows Kondo impurity-like behaviour up until* $x = 0.2$. *Lattice coherence effects become important for higher values of* x.

The application of Kondo disorder models to explain heavy-fermion NFL alloys was motivated by the observation of broad NMR and μSR lines in $UCu_{5-x}Pd_x$ (x=1.0 and 1.5). These large linewidths are unambiguously due to static disorder, since the separately measured dynamic lifetime broadening is much less than the observed widths, and indicate the presence of an inhomogeneous distribution of the static spin polarization associated with the U ions. Zero-field μSR experiments on a number of NFL alloys show no static magnetic moment greater than $0.01\mu_B$/f ion, so the spin polarization is paramagnetic in origin and not due to static magnetism associated with the antiferromagnetic or spin-glass freezing of the U-ion spins [15].

Fig. 3.4 [9] focusses on the x=0.2 resistivity curve from Fig. 3.3, where the behaviour is decidedly impurity-like. But even at the lowest temperatures (inset), $\rho(T)$ is linear and there is no indication of a return to quadratic scattering. This, along with the logarithmically divergent $\gamma(T)$ (Fig. 3.2) suggests that the system is metallic but not a Fermi liquid.

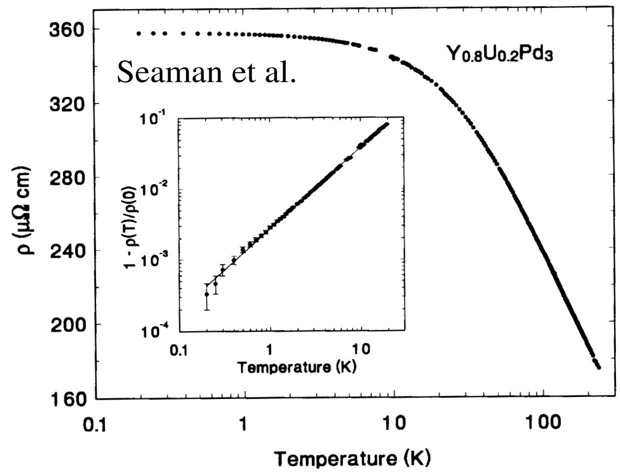

Figure 3.4: *$\rho(T)$ vs. T for x=0.2. There is a Kondo-like log-linear regime around 80-100K. At low temperatures, the resistivity becomes linear (inset), suggesting a non Fermi-liquid ground state.*

We find further evidence of the NFL ground state from optical conductivity measurements. In Fig. 3.5 and 3.6 [10], experimental results for the real part of the optical conductivity (σ_1) and the transport relaxation rate $\Gamma(\omega)$ are plotted. The relaxation rate is related from $\sigma(\omega)$ by

$$\sigma(\omega) = \frac{(\omega_p)^2}{4\pi} \frac{1}{\Gamma(\omega) - \imath\omega(1+\lambda(\omega))} \tag{3.1}$$

and represents the quasiparticle scattering rate for a Fermi-liquid. Similarly, for a Fermi-liquid, $1+\lambda(\omega)$ is the effective mass m^*. In the far-infrared region ($\omega \leq 100cm^{-1}$), σ_1 decreases with decreasing temperature, while it is temperature independent at high frequencies. This is obviously in accordance with the increasing resistivity with decreasing temperature. At $300K$, σ_1 is basically Drude-like up to the mid-infrared spectral range, consistent with the constant $\Gamma(\omega)$ (Fig. 3.6).

In Fig. 3.6, $\Gamma(\omega)$ in the far-infrared region is fit to a linear form in ω and T at low temperatures. Since for a Fermi-liquid at low T, $\Gamma(\omega) = -2\mathrm{Im}\Sigma(\omega/2)$, one might expect the same functional behaviour here for $\Gamma(\omega)$ and $\rho(T)$ and they are indeed both linear at low energies.

For a theoretical understanding of how the non-Fermi liquid originates in the heavy fermions, one needs to handle correlated lattice systems under some approximation scheme. The one we employ is a particular kind of mean field approximation where the lattice problem is reduced to an Anderson impurity coupled to a time-dependent effective field. This impurity problem can then be solved using Quantum Monte Carlo techniques. We discuss these methods of solution in the next chapter.

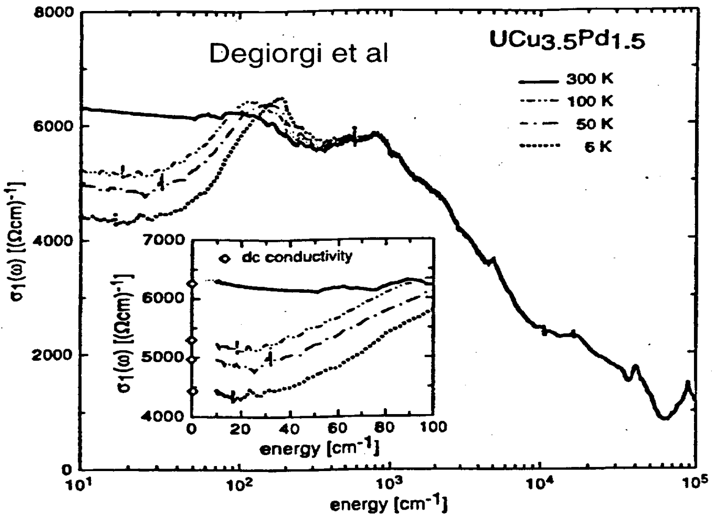

Figure 3.5: *Optical conductivity σ_1 measurements show the absence of a Drude peak at low T, evidenced in the linear optical scattering rate $\Gamma(\omega)$. As T is increased, a zero frequency peak emerges.*

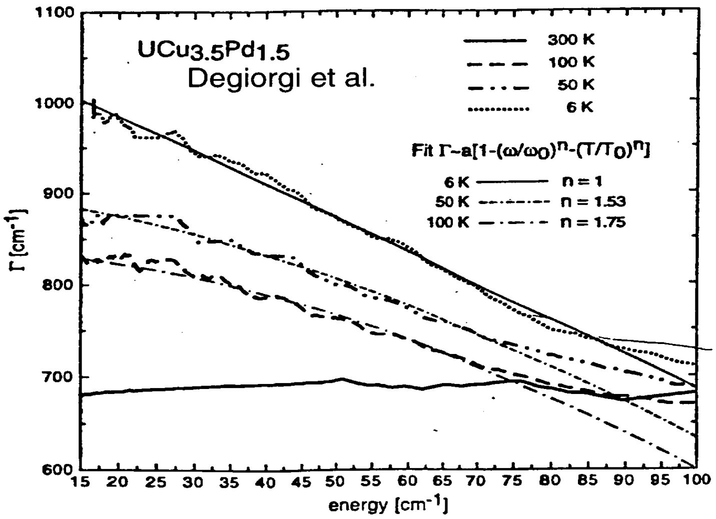

Figure 3.6: $\Gamma(\omega)$ *is fit to a sequence of functions with increasing temperature. At the lowest temperatures, it is linear in ω and T, indicating a non-Fermi. At 100K, one recovers a quadratic relaxation rate.*

Chapter 4

Models and Methods of Solution

4.1 Limit of Infinite Spatial Dimensions

In 1989, Metzner and Vollhardt developed a new approach to study strongly correlated lattice models[17] based on an expansion in inverse dimensionality $1/D$ about the limit $D = \infty$. In this limit, strong local interactions like the screened Coulomb repulsion in the models remain nontrivial while interactions like non-local spin-exchange essentially reduce to the corresponding mean-field result [18]. The use of $D = \infty$ limit brings a few profound simplifications into the physical problem which we will describe in the following.

On a hypercubic lattice, each site has $2D$ nearest neighbors, $2D(D-1)$ next nearest neighbors, etc. The fluctuations produced at a given site due to interactions with its nearest neighbors is an effect of order $1/D$ and may be neglected when D is large. Thus, the large D hypercubic lattice is a natural venue for developing a mean-field theory.

The non-interacting density of states of a tight binding type model in the limit of $D = \infty$ has a Gaussian form in energy. The origin of the Gaussian bare density of states can be understood from arguments[17] based on the central limit theorem. Each direction in the infinite-dimensional Brillouin zone contributes independently to the density of states. The mean square energy contributed by each direction is $2t^2$. Thus, with D independent directions, the bare density of states is a Gaussian

$$\rho^0(\epsilon) = \sqrt{\frac{1}{4t^2 d\pi}} \exp -\epsilon^2/4t^2 D \tag{4.1}$$

with width $2\sqrt{Dt^2}$. This must remain finite as $D \to \infty$ in order for the bare electron energy to remain finite. This can only happen if Dt^2 remains a constant as $D \to \infty$. Typically, one uses this to define a unit of energy $t^* = 2t\sqrt{D} = 1$. It is interesting to note that the constancy of t^* as $D \to \infty$ also insures that the magnetic properties of Hubbard-like models to remain nontrivial. In a mean-field based theory we expect that transition temperature to go roughly as the net magnetic exchange between any site and its set of $2D$ nearest neighbors, $2DJ \sim -4Dt^2/U$ which remains finite as $D \to \infty$.

Metzner and Vollhardt [17] observed that the irreducible self-energy and vertex-functions become purely local as the coordination number of the lattice increases. The locality of the self energy (i.e. its momentum independence) can be understood from simple diagrammatic arguments. The single-particle Green's functions $G(R, i\omega_n) \sim t^R$ to leading order in the hopping integral t, thus they fall off very quickly with distance in the large D limit, $G(R, i\omega_n) \propto D^{-R/2}$, so that nonlocal diagrams in the

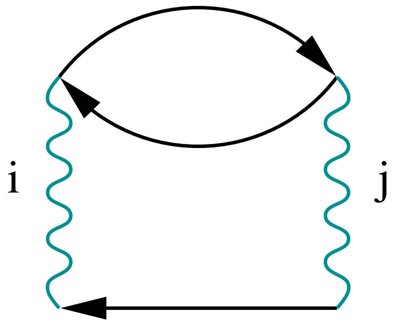

Figure 4.1: *Second order contribution to the self energy of the Hubbard model. Here, the solid lines represent the undressed ($U = 0$) electron propagators $G^0_{ij}(i\omega_n)$, and the dashed lines represent the intra-site interaction U. If sites i and j are nearest neighbors, then this diagram scales like $t^3 \sim 1/D^{3/2}$ which vanishes when $D \to \infty$. Only the local contribution $i = j$ survives.*

irreducible self energy (and two-particle irreducible vertices) may be neglected. For example, consider the second order Hubbard self energy diagram shown in Fig. 4.1. If sites i and j are nearest neighbors, then this contribution to the self energy scales like $t^3 \sim 1/D^{3/2}$ which vanishes in the infinite-dimensional limit. In fact, the contributions from the next nearest neighbor shell, etc. also vanish. The only contribution which survives in the infinite-dimensional limit is the local one for which $i = j$. Thus, the self energy for the single-particle Green's function and the irreducible vertex functions have no momentum dependence and are functionals of the local Green's function [17] and the interaction.

4.2 Dynamical Mean Field Approximation

The dynamical mean field approximation (DMFA) casts the lattice problem into a single correlated site positioned in a "mean field" produced by the neighboring sites. In doing so, the DMFA freezes all spatial fluctuations just like the usual mean-field approach ; however, unlike the usual mean-field theory, here the "mean field" is a function of time instead of being a pure number. In fact the "dynamical mean field" is the probability amplitude for creating particle on the site at given time and destroying it back to the host at a later time. In this way the DMFA retains the important quantum (temporal) fluctuation of the original problem, hence the adjective "Dynamical". Like any mean field theory this approximation works better as the coordination number increases, or equivalently as the number of spatial dimensions increases.

The basic idea of the DMFA is to map the lattice model onto a corresponding self-consistently embedded Anderson impurity model. The self-energy of the lattice problem become purely local (momentum independent) as the number of nearest neighbors to a given site, or equivalently the number of spatial dimensions, goes to infinity[17]. So, if we know the self-energy of the single impurity Anderson model (which is inherently local) we can assume that it is the approximate self-energy for the corresponding lattice model in $D = \infty$. In fact, to make this assumption work, the correspondence between the two models should be determined self-consistently as displayed in Fig. 4.2. Given a guess for the *host* Green's function $\mathcal{G}$, we use the QMC procedure to solve the corresponding single impurity problem. The resulting Σ is then

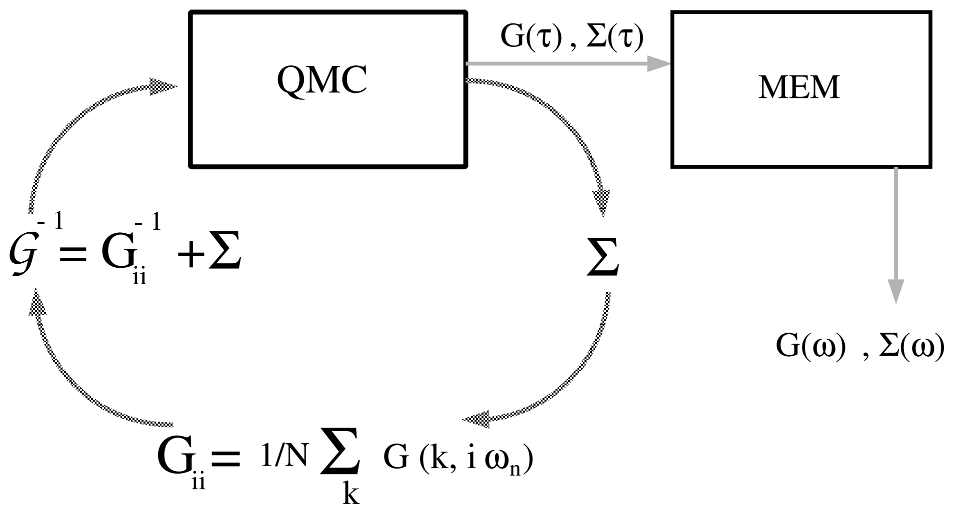

Figure 4.2: DMFA algorithm.

used to find a local Green's function for the lattice problem via $G_{ii}(z) = \frac{1}{N}\sum_k G_k(z)$ where $G_k(z)$ has the appropriate functional form in terms of Σ for the particular lattice model. By subtracting off the local self energy from $G_{ii}(z)$, we get a new $\mathcal{G}$ which is used to reinitialize the process.

The introduction of $\mathcal{G} = [G_{ii}^{-1} + \Sigma]^{-1}$ is necessary to avoid over-counting diagrams on the site i. The first few terms of the diagrammatic series for the Hubbard model self energy is shown in Fig. 4.3. This is the same diagrammatic series as that for the self energy of the Anderson impurity model; however, in order to not over-count the local self energy (c.f. the third order in U diagram) it is necessary to subtract the local self energy from the local propagator $\mathcal{G}$ which defines the solid line. $\mathcal{G}(\imath\omega_n)^{-1} = G(\imath\omega_n)^{-1} + \Sigma(\imath\omega_n)$, where $G(\imath\omega_n) = G(R=0, \imath\omega_n)$ is the full local Green's function. Thus, the self energy of the infinite-dimensional Hubbard model is a functional of

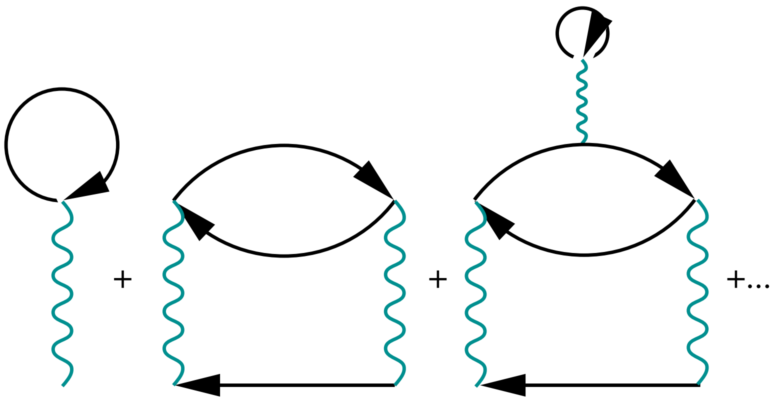

Figure 4.3: *First few diagrams for the self energy of the infinite-dimensional Hubbard model. Note that this is the same diagrammatic series as that for the self energy of the Andersen impurity model, but to avoid over-counting the local self energy (c.f. the third order in U diagram) it is necessary to subtract the local self energy to define the local propagator $\mathcal{G}$ represented by the solid line, $\mathcal{G}(i\omega_n)^{-1} = G(i\omega_n)^{-1} + \Sigma(i\omega_n)$, where $G(i\omega_n) = G(R = 0, i\omega_n)$*

the site-excluded Green's function and the local interaction $\Sigma(\mathcal{G}, U)$; it has the same diagrammatic expansion as an Anderson impurity with local interaction U and local (host) Green's function $\mathcal{G}(\imath\omega_n)$, given by $\mathcal{G}(\imath\omega_n)^{-1} = G(\imath\omega_n)^{-1} + \Sigma(\imath\omega_n)$. In contrast to the standard skeleton perturbation theory, the QMC yields an exact solution to all orders in U, and thus it is necessary to subtract off the interaction on the site where Σ is calculated. This whole process is repeated until convergence is reached.

4.2.1 DMF for a dilute system

Let us imagine a lattice where a small fraction x of the sites are correlated (call these sites A) and $(1-x)$ of them are uncorrelated (call them B). The Green's functions for these two kinds of sites can be written as

$$G_A^{-1} = \mathcal{G}^{-1} - \Sigma; G_B^{-1} = \mathcal{G}^{-1} \tag{4.2}$$

where $\mathcal{G}$ is the effective medium. Then we can write the average Green's function $\overline{G}$ as

$$\begin{aligned} \overline{G} &= xG_A + (1-x)G_B \\ &= x(\mathcal{G}^{-1} - \Sigma)^{-1} + (1-x)\mathcal{G} \\ &= \mathcal{G} + \mathcal{G}\frac{x\Sigma}{1-\Sigma\mathcal{G}}\mathcal{G}\,. \end{aligned} \tag{4.3}$$

From this we can identify the average t matrix as

$$\bar{t} = \frac{x\Sigma}{1-\Sigma\mathcal{G}}\,; \tag{4.4}$$

now writing the Dyson's equation for $\overline{G}$ in terms of an average self-energy

$$\overline{G} = \mathcal{G} + \mathcal{G}\overline{\Sigma}\overline{G} \tag{4.5}$$

one can relate this self-energy to the t-matrix

$$\overline{\Sigma} = \frac{\bar{t}}{1+\bar{t}\mathcal{G}} \tag{4.6}$$

In Chap. 5, we use this relation to calculate the conduction electron self-energy from the impurity t-matrix in Eq.(5.3).

4.3 The Method of Quantum Monte Carlo

We saw that by using DMFA a strongly correlated lattice problem can be mapped to a self-consistently embedded single impurity problem which is generally expressed by the Anderson impurity Hamiltonian $H = H_0 + H_I$, where

$$\begin{aligned} H_0 &= \sum_{\mathbf{k},\sigma} \epsilon_{\mathbf{k}} n_{\mathbf{k},\sigma} + V \sum_{\mathbf{k},\sigma} \left(d^{\dagger}_{\mathbf{k},\sigma} f_{\sigma} + \text{H.c.} \right) \\ &+ \left[\epsilon_f + \frac{U}{2} \right] \sum_{\sigma} n_{f,\sigma} \end{aligned} \tag{4.7}$$

and

$$H_I = U \left[n_{f\uparrow} n_{f\downarrow} - \frac{1}{2} \left(n_{f\uparrow} + n_{f\downarrow} \right) \right] . \tag{4.8}$$

Hirsch and Fye [19] developed an algorithm to solve this impurity problem based on a Monte Carlo sampling of the phase space. We will sketch this algorithm and refer the reader to the original paper [19] for details.

The Hamiltonian H defines a quantum many particle problem with a partition function $Z = Tre^{-\beta H}$ in temperature $T = 1/\beta$, where the trace is to be taken over all Fermionic variables. We write the partition function in the Trotter approximation as

$$Z = Tre^{-\beta H} \cong Tr \left[\prod_{l=1}^{L} e^{-\Delta\tau H_0} e^{-\Delta\tau H_I} \right] , \tag{4.9}$$

with $\Delta\tau = \beta/L$ denote the imaginary time slices. In the Trotter decomposed Z, the errors committed are of $O(\Delta\tau^2)$ and can be minimised by making $\Delta\tau$ small.

The first exponential in Z is quadratic in fermion variables and can be easily integrated out. The interaction term H_I is quartic in fermions and can be decoupled at each time slice l using the discrete Hubbard-Stratanovich transformation (where the auxiliary fields are Ising variables s_l)

$$e^{-\Delta\tau H_I} = \frac{1}{2}\sum_{s=\pm 1} e^{\lambda s(n_{f\uparrow}-n_{f\downarrow})} \tag{4.10}$$

where $\cosh(\lambda) = e^{\Delta\tau U/2}$. Now the action is entirely quadratic and a trace over the fermions yields

$$\begin{aligned} Z &\approx \left[\prod_{k,\sigma}\det\left({g^0_{k,\sigma}}^{-1}(\tau_l,\tau_{l'})\right)\right]\left[Tr_{\{s_l\}}\prod_{\sigma=\pm 1}\det\left(O_{f,\sigma}[s_l]\right)\right] \\ &= Z_{cond.}Tr_{\{s_l\}}\left[\det\left(O_{f,\uparrow}[s_l]\right)\det\left(O_{f,\downarrow}[s_l]\right)\right] . \end{aligned} \tag{4.11}$$

Z_{cond} is the contribution from the non-interacting conduction band Green's function $g^0_{k,\sigma}$ and $O_{f,\mu}$ is the inverse of the impurity Green's function

$$g_{f,\mu} = O^{-1}_{f,\mu} . \tag{4.12}$$

The matrix elements of $O_{f,\mu}$ at each time slice l are of the type $e^{V^\mu_l}$, where V is a potential acting at the impurity site given by

$$V^\mu_l = \lambda\mu s_l \left|f\right\rangle\left\langle f\right| . \tag{4.13}$$

4.3.1 QMC updating

While outlining the Monte Carlo updating procedure, we often drop the time, spin and species indices on $g_{f,\mu}$ and $O_{f,\mu}$, for convenience.

Given two arbitrary Ising configurations s and s' that give rise to the impurity potentials V and V' (dropping the time and spin indices), the impurity Green's functions follow the Dyson equation

$$g' = g + (g - I)(e^{V'-V} - I)g' \,. \tag{4.14}$$

Multiplying through by g'^{-1}, we get

$$gg'^{-1} = I + (g - I)(I - e^{V'-V}) \,. \tag{4.15}$$

From Eq. 4.11, we can easily infer that the relative weight of these two configurations s and s' is given by

$$\begin{aligned} \frac{\det O'}{\det O} &= \det(gg'^{-1}) \\ &= \det\left[I + (I - g)(e^{V'-V} - I)\right] \,. \end{aligned} \tag{4.16}$$

To evaluate this determinant, we use the following matrix identity

$$\begin{aligned} \det(I + A) &= e^{Tr\ln(I+A)} \\ &= I + TrA + \frac{1}{2}\left[(TrA)^2 - (TrA^2)\right] + \ldots \,. \end{aligned} \tag{4.17}$$

In this case, however, $A = (I - g)(e^{V'-V} - I)$ is a matrix that has non-zero entries in one column only. Therefore $(TrA)^n = Tr(A^n)$, which cancels the higher order terms; and we have for each time slice l

$$\begin{aligned} R_\mu^l &= \frac{\det\left(O_\mu[s_l']\right)}{\det\left(O_\mu[s_l]\right)} \\ &= Tr\left[I + (I - g)(e^{V'-V} - I)\right] \\ &= 1 + [1 - g^\mu(l,l)]\left(e^{V_l'^\mu - V_l^\mu} - 1\right) \,. \end{aligned} \tag{4.18}$$

Let us consider the symmetric Anderson impurity model which corresponds to setting $\epsilon_f + \frac{U}{2} = 0$ in Eq. 4.7. Here because of particle-hole symmetry, the product $R^l = R^l_\uparrow R^l_\downarrow$ is always positive. An elemental Monte Carlo move corresponds to proposing a spin-flip ($s_l \to s'_l = -s_l$) and if R^l is greater than a random number between 0 and 1, the move is accepted; otherwise, it is rejected. If the move is accepted, the impurity Green's function for the new configuration is obtained from the old one through the relation

$$g'(l_1, l_2) = g(l_1, l_2) + \left[\frac{[g(l_1, l) - \delta_{l_1,l}]\,(e^{V'_l - V_l} - 1)}{R^l} \right] g(l, l_2)\,, \tag{4.19}$$

which follows from Eq. 4.14. For this model, we start with the $U = 0$ Green's function for the impurity site

$$\mathcal{G}(l, l') = \frac{1}{\beta} \sum_n e^{-\imath\omega_n(\Delta\tau)(l-l')} \mathcal{G}(\imath\omega_n) \tag{4.20}$$

where $\omega_n = (2n+1)\pi/\beta$ and

$$\mathcal{G}(\imath\omega_n) = -\frac{1}{\imath\omega_n - \imath\Delta sgn(\omega_n)}; \Delta = \pi N(E_F)V^2 \tag{4.21}$$

and build in correlations sequentially.

The case is a bit different for a correlated lattice. Here, since the bare Green's function $\mathcal{G}$ is not *a priori* known, the QMC algorithm must be iterated as shown in Fig. 4.2 to determine a self-consistent solution for the Green's function of the infinite-dimensional lattice. This process is repeated until convergence is reached.

4.4 Maximum Entropy method

Most quantum Monte Carlo (QMC) simulations produce Green's functions $G(\tau)$ of imaginary time $\tau = it$. The knowledge of $G(\tau)$ in the range $0 \leq \tau \leq \beta$, where $\beta = 1/k_B T$, is complete because $G(\tau)$ is periodic for Bosons and antiperiodic for Fermions. However, real-frequency results are crucial to obtain since most experiments probe dynamical quantities like transport, density of states, nuclear magnetic resonance, inelastic scattering, etc. The relation between $G(\tau)$, and $A(\omega) = -\frac{1}{\pi}\mathrm{Im}G(\omega)$ is linear and surprisingly simple, for example for a Fermionic single-particle Green's function G

$$G(\tau) = \int d\omega \frac{A(\omega) e^{-\tau\omega}}{1 + e^{-\beta\omega}} . \tag{4.22}$$

The QMC calculations provide data, $G(\tau_l)$ (i.e., calculated at a discrete set of τ points $\{\tau_l\}$, distributed in the range $0 \leq \tau \leq \beta$), which are incomplete and noisy (i.e., subject to statistical error). In this case, the inversion is ill posed because there exist an infinite number of A that can yield the same G. In other words, for finite τ and large ω the kernel is exponentially small, thus $G(\tau)$ is insensitive to the high frequency features of $A(\omega)$. Hence, if we approximate both G and A by equal-length vectors and K by a square matrix, then we find that the determinant of K is exponentially small, so that K^{-1} is ill-defined. In fact the non-invertibility of the above relation is one of the biggest and ever-lasting problems in pure mathematics. Had we known how to invert this relation analytically, we could have used it to find solutions for many differential equations which are formidable to solve in the original variable space (t or ω) but can be easily solved in the corresponding Euclidean space (τ).

Clearly we need a numerical method to do the above inversion. We employ the Maximum Entropy Method (MEM) for this purpose. In very simple words, MEM presents a way to choose the most probable $A(\omega)$ from among the large number of possibilities. Here we try to sketch the essentials of this method briefly and refer the reader to review articles [21, 22] for details.

MEM is based on the Bayesian statistics which handles the conditional probabilities, i.e., $P[X|Y]P[Y] = P[Y|X]P[X]$ where $P[X|Y]$ is the conditional probability of X given Y. To specialize this to the analytic continuation problem, we introduce three quantities. The first is the probability distribution of $A(\omega)$ (image) before the experiment (QMC simulation) is conducted, $P[A(\omega)]$, called the "prior probability". The second is the conditional probability of producing the data, $G(\tau_l)$, via the experiment for a given $A(\omega)$, which is termed the "likelihood function" $P[G(\tau)|A(\omega)]$. The third is the conditional probability of $A(\omega)$ given the data after the experiment, $P[A(\omega)|G(\tau)]$, which is called the "posterior probability". The probability distribution of the data, $P[G(\tau)]$, is a constant during one experiment and may be ignored. So Bayes' theorem states that

$$P[A(\omega)|G(\tau)] \sim P[G(\tau)|A(\omega)]P[A(\omega)]. \tag{4.23}$$

MEM postulates that the *image* to be presented, $A_I(\omega)$, is the $A(\omega)$ which maximizes the posterior probability.

The likelihood function contains the new information provided by the experiment. If the data, $G(\tau_l)$ are assumed to be independent and Gaussian distributed with error σ_l, the likelihood function tells how well the image can be fitted to the data according to a Gaussian distribution,

$$P[G(\tau)|A(\omega)] \sim \exp(-\chi^2/2), \tag{4.24}$$

where

$$\chi^2 = \sum_l \frac{[G(\tau_l) - G_f(\tau_l)]^2}{\sigma_l^2}, \tag{4.25}$$

where $G_f(\tau_l)$ are the data that the given $A(\omega)$ would produce in the absence of noise, i.e., the $G(\tau)$ produced from $A(\omega)$ from Eq. 4.22. If, at this stage, one assumes that the prior probability is a constant, then maximizing the posterior probability is equivalent to fitting the data by the method of least squares, i.e., minimizing χ^2.

The maximum entropy method corresponds to a particular choice of the prior which incorporates the prior knowledge of positivity and additivity of the spectral function. A variety of different statistical inference arguments [22] lead to the conclusion that the prior should take the form

$$P[A(\omega)] \sim \exp(aS). \tag{4.26}$$

Here, S is the information theory entropy [23] of the image

$$S = \sum_i \Delta\omega \left[A(\omega_i) - m(\omega_i) - A(\omega_i) \ln \left[\frac{A(\omega_i)}{m(\omega_i)} \right] \right]. \tag{4.27}$$

S is defined relative to a starting model, $m(\omega)$, for $A(\omega)$. It is termed the *default model*, because it is the image to which the MEM will default in the absence of data.

It is usually chosen to be the smoothest function consistent with prior knowledge such as sum rules.

Finally, the image is obtained by maximizing the posterior probability. This is equivalent to a functional variation of $A(\omega)$ to maximize the entropy S, subject to a constraint on χ^2 with a Lagrange multiplier $1/a$; hence the name maximum-entropy method. $1/a$ controls the relative importance of the prior and the data. Before the experiment the image starts at the default model and $a = \infty$. As the data improve a becomes smaller, and the image deviates from the default model towards the correct $A(\omega)$. Now, it remains to have a "stopping criteria" for obtaining the final image since the correct $A(\omega)$ is not a-priori known. In the traditional (*historic*) use of MEM, $1/a$ is chosen so that the image maximizes the entropy subject to the condition that it fits the data according to $\chi^2 \leq N_\tau$, where N_τ is the number of independent data samples (bins). In the more modern (or *classic*) MEM, $1/a$ is itself determined by Bayesian arguments that maximizes the posterior probability of a given the data, $P[a|G(\tau)]$.

The most important physical part involved in the above sketch of MEM is choosing the default model to begin with. For example, people usually choose the default model according to the perturbation approximation of $A(\omega)$. Occasionally we have reason to calculate a series of spectra for a variety of temperatures. If these temperatures are sufficiently close to each other, then starting from a perturbation theory default at the highest temperature, we can use the resulting spectra as a default model for the next lower temperature (we call this the *annealing* method). The *annealing* method may not have a Bayesian justification, but it has an important physical motivation. At sufficiently high temperatures the perturbation results are known to be very accurate. Thus, the annealing procedure may start with a very good default model. At lower temperatures, the QMC is known to work better except for the large frequency tails (which are again taken care of by using perturbation tails in their place). The data gets gradually more structure as temperature is lowered, hence there is no reason to believe that annealing introduces excessive information into the prior for lower temperature as is certainly true for the reverse process (i.e., feeding the image of a lower T as the default).

Chapter 5

Non Fermi liquid dynamics of disordered heavy fermions

Ref: A. Chattopadhyay and M. Jarrell, *Dynamics of disordered heavy-fermion systems*, Phys. Rev. B, **56**, R2920 (1997) [Rapid Communications].

5.1 Introduction.

Over the past four decades, the Fermi-Liquid paradigm has been the key to our understanding of metallic behavior. In Fermi-liquid theory we assume a 1:1 correspondence between the low-lying eigenstates of the interacting system to those of the noninteracting electron gas. This leads to a magnetic susceptibility that is weakly temperature dependent, a specific heat linear in T, and a low temperature resistivity that is quadratic.

However, recently there has been a great deal of experimental interest in disordered heavy-Fermion compounds[8] (e.g.$Y_{1-x}U_xPd_3$, $UCu_{5-x}Pd_x$), where strong electronic correlations preclude Fermi-liquid behavior. The non Fermi-liquid behavior in these compounds is characterized by a linear resistivity at low T, a logarithmic low temperature divergence of the susceptibility and the specific heat coefficient, an optical conductivity with a low frequency pseudogap and a linear transport scattering rate at low frequencies [8, 10, 11]. Several models have been proposed to explain these experimental results. Among them are theories based upon proximity to a zero temperature quantum critical point[12] and those which explain the impurity to lattice crossover effects in the multi-channel Kondo model[13].

Dobrosavljević et al.[14] investigated a dilute system of magnetic impurities in a disordered metal. Since disorder can give rise to a distribution of the local density of states of the conduction electrons, a distribution of Kondo scales $P(T_K)$ is induced that could be singular enough to produce χ and γ that diverge as $T \rightarrow 0$, a strongly non-Fermi-liquid behavior. More recently, Bernal et al.[15] have shown that this $P(T_K)$ is not appropriate for the U-doped heavy-Fermion systems. They propose an alternative spread of Kondo scales, and use it to calculate the thermodynamics of these alloys. Miranda, et al.[20] have recently shown that the underlying mechanism behind the non-Fermi liquid transport and thermodynamics is the presence of a finite number of unquenched low-T_K spins, along with an essentially constant $P(T_K)$ at low T_K. This gives a linear in T low temperature resistivity.

5.2 Formalism.

We stay within this phenomenological framework and calculate dynamical quantities such as the optical conductivity and self-energy. Our analysis is strictly valid only in systems with a *dilute* collection of Kondo centers, like $Y_{1-x}U_xPd_3$, but the leading frequency dependence of the dynamical quantities (at low T) should apply to concentrated systems like $UCu_{3.5}Pd_{1.5}$ as well[24]. We begin by concentrating on the Kondo regime of the Anderson impurity model, where d-electrons occupy the conduction band, and f-electrons provide the magnetic impurities for the spin-spin scattering processes. In the low temperature limit this model corresponds precisely to the Fermi-liquid picture of Landau. The electronic density of states has a resonance at the Fermi level, giving significant impurity contributions to the specific heat and magnetic susceptibility. Following Doniach and Sunjic[25], Frota and Oliveira[26] argued that the Doniach-Sunjic form, modified to account for the $\pi/2$ phase shift, should describe the shape of Kondo resonance. Their expression is in agreement with their results for the Kondo resonance obtained from numerical renormalization group calculations[4], as well as low-temperature quantum Monte Carlo (QMC) results analytically continued with the Maximum Entropy method (MEM)[21, 22].

We can generalize their expression to finite temperatures and get

$$A_f(\omega, T_K) = \frac{1}{\pi\Delta}\mathrm{Re}\left[i\Gamma_K/(\omega + i\sqrt{\Gamma_K^2+\gamma^2})\right]^{1/2}, \tag{5.1}$$

where Δ is the f-d hybridization energy, and $\Gamma_K = (\pi/2)^2 T_K$ is the half-width of this resonance, T_K being the Kondo temperature. We add a temperature dependent width γ to the original expression of Frota and Oliveira[26], with γ determined by fitting to QMC-MEM results[21]. As shown in Fig. 5.1, this form continues to exhibit remarkable agreement with the shape of the Kondo resonance (the low-frequency peak) obtained from QMC-MEM, *even at finite temperatures*. By comparison with a wide range of Anderson impurity spectra, we were able to obtain the universal function $\gamma(T/T_K)$ for over three decades of T/T_K. For $T/T_K \leq 0.3$, we use $\gamma(T) = 4.52T$, a value derived from Noziéres'[27] phenomenological Fermi-liquid description of the Kondo problem at low temperatures.

Since we are working in the dilute limit, we assume the impurities to be independent scatterers and disorder average over the universal single impurity spectral function (eq.1) to calculate dynamical quantities. The Hilbert transform of $A_f(\omega, T_K)$ then gives the average impurity t-matrix

$$t_f(z) = \int dT_K P(T_K) \int d\omega \frac{V^2 A_f(\omega, T_K)}{z - \omega}\,, \tag{5.2}$$

where V is the f-d hybridization. Following Miranda, et al.[20] we use a dynamical mean-field approximation[17], which becomes exact in the limit of infinite dimensions, to calculate the lattice self energy from a concentration x of substitutional Kondo impurities

$$\Sigma(\omega) = \frac{x t_f(\omega)}{1 + x t_f(\omega) \mathcal{G}(\omega)}\,, \tag{5.3}$$

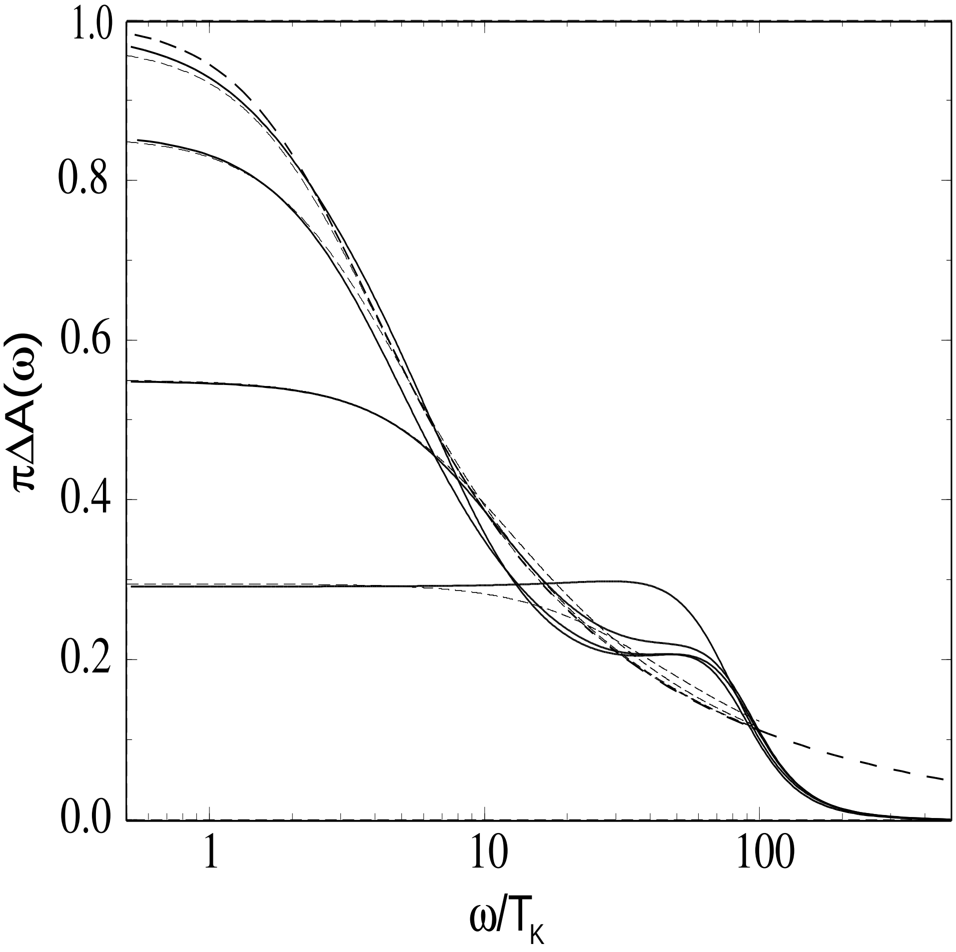

Figure 5.1: *Spectral function for the f-electron in the Kondo limit of the Anderson model. The long-dashed line is the Doniach-Sunjic result[26] (true for $T = 0$). The dotted lines represent the extension of the Doniach-Sunjic result to finite T which is used for calculating the dynamics in this chapter; the solid lines represent QMC-MEM results.* T/T_K *= 0.2, 0.8, 3.2 and 12.8 for the curves from top to bottom. For* $T/T_K \leq 0.3$, $A_f(\omega, T_k)$ *has a width* $\gamma = 4.52T$ *which comes from Fermi-liquid theory[27]. For higher* T/T_K, *we adjust* γ *to fit the QMC-MEM data.*

where $\mathcal{G}(\omega)$ describes the average effective medium of the impurity (Eq. 4.6). It is related to the average local host greens function G

$$G(\omega) = \int d\epsilon \frac{N(\epsilon)}{\omega - \epsilon + \mu - \Sigma(\omega)}\,, \tag{5.4}$$

through the relation

$$\mathcal{G}^{-1} = G^{-1} + \Sigma\,, \tag{5.5}$$

where $N(\epsilon) = \frac{1}{t^*\sqrt{\pi}} e^{-\epsilon^2/t^{*2}}$ and we set $t^* = 10,000K$ to establish a unit of energy and temperature. The solutions of Eqns. 1–5 then give the full lattice self energy.

The knowledge of this self energy enables one to calculate physical quantities[28] like transport coefficients and the optical conductivity. In this chapter we concentrate on the optical conductivity $\sigma(\omega)$. It is measured in units of $\sigma_0 = e^2\pi/2\hbar a$, which with $h/e^2 \approx 2.6 \cdot 10^4\Omega$, varies between $10^{-3}...10^{-2}[(\mu\Omega cm)^{-1}]$, depending on the lattice constant a.

5.3 Results

We choose three different distributions $P(T_K)$, corresponding to strong[14], weak[15] and a phenomenological disorder motivated by Miranda et al.'s[20] argument that the experimental $P(T_K)$ should be relatively constant at low temperatures. We consider the distribution of Kondo scales as arising from a distribution of couplings between the conduction and the f-electron spins $P(J)$. For the strongly disordered sample,

$P(T_K)$ has the form[14]

$$P_{sd}(T_K) = (4\pi)^{-1/2}\frac{1}{T_K\ln(t^*/T_K)}\times \exp\{-0.25\ln^2[0.217e^{-1}\ln(t^*/T_K)]\}\,, \tag{5.6}$$

where we have used a bulk Kondo temperature $T_K^0 = 10^2K$ (in most U-based HF systems $T_K^0 = 10^2K$ varies between 100-200 K). The weak disorder is characterized by a Gaussian distribution $P(J)$ of width $2u = 0.01$, where u is a disorder parameter [14] and a higher value of u corresponds to more disorder. This leads to

$$P_{wd}(T_K) = \frac{1}{\sqrt{0.01\pi}}\frac{1}{0.217T_K\ln^2(T_K/t^*)}\times \exp\left\{-100\left[\frac{1}{0.217\ln(T_K/t^*)}+1\right]^2\right\}. \tag{5.7}$$

For the phenomenological spread of Kondo scales, we assume the form

$$P_{ph}(T_K) = \frac{0.01}{e^{(T_K-T_K^0)}+1}\,. \tag{5.8}$$

This distribution is not based on microscopics; it simply satisfies the experimental criterion of constancy at low T_K and looks qualitatively similar to the $P(T_K)$ for $UCu_{5-x}Pd_x$[20]. Unlike the $1/(T_K\ln T_K)$ divergence of the strongly disordered case, $P_{ph}(T_K)$ has a finite number of spins with $T_K = 0$.

The nature of the disorder gives rise to different physics in each case, as is manifested in the functional form of $\mathrm{Im}\Sigma(\omega)$ [Fig. 5.2] (these plots are for $T = 0$ and $x = 0.2$ for all three distributions).

For a weakly disordered system, $\mathrm{Im}\Sigma(\omega)$ has the form $-c+\omega^2$ as $\omega \to 0$ where c is a constant[30]. This suggests a finite lifetime for the electrons at the Fermi energy at

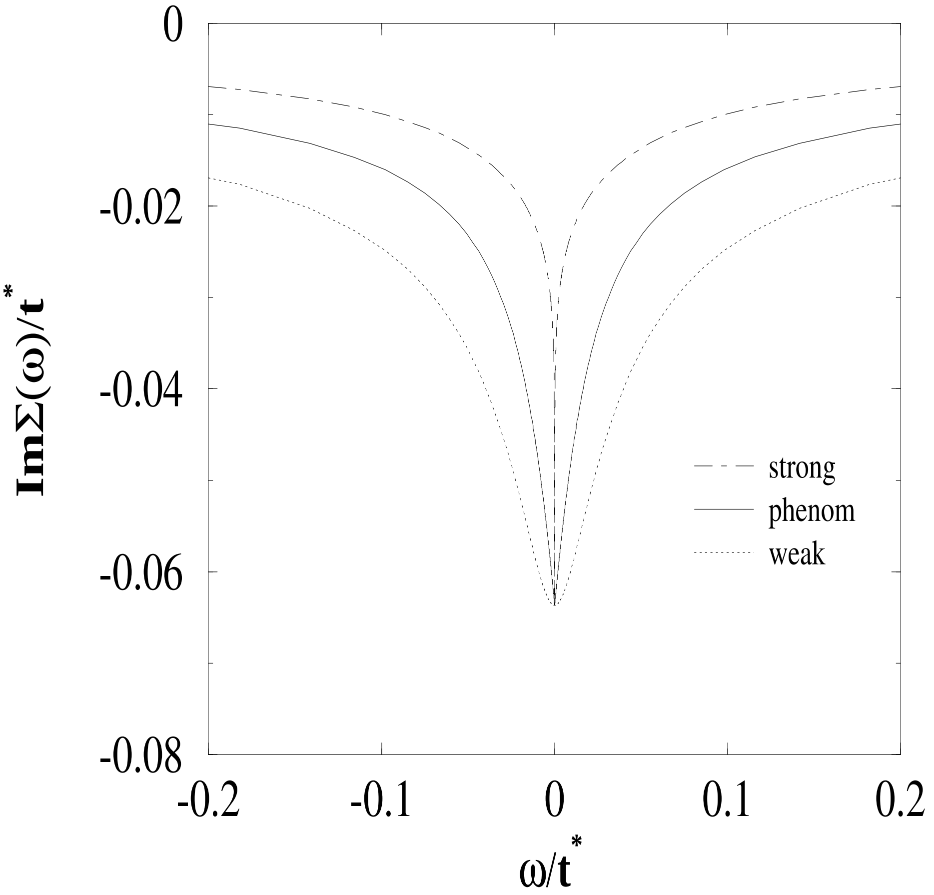

Figure 5.2: *Imaginary part of the conduction electron self energy when* $T = 0$ *and* $x = 0.2$*. The three different curves denote different distributions of disorder. The lowest one corresponds to very weak disorder (*$P(T_K) \to 0$ *as* $T_K \to 0$*) and at low* ω *has the form* $\mathrm{Im}\Sigma(\omega) \propto -c + \omega^2$*, giving a local Fermi liquid with* $\rho(T) = \rho(0) - AT^2$*. The highest one is for strong disorder (still metallic), with a* $\omega^{1/4}$ *dependence as* $\omega \to 0$*. The one in the middle corresponds to a phenomenological distribution of Kondo scales suitable for the heavy-fermion systems. It approaches the form* $\mathrm{Im}\Sigma(\omega) \propto -c + |\omega|$ *as* $\omega \to 0$*. This strongly hints towards a linear resistivity at low* T *in these compounds.*

zero temperature which makes it different from a normal (pure metal) Fermi liquid. But since there are no unquenched spins at $T = 0$, the system does form a local Fermi liquid, with a resistivity $\rho(T) \sim \rho(0) - AT^2$. For the case of strong disorder, $P_{sd}(T_K)$ is divergent at low T_K. Even though we are on the metallic side of the metal-insulator transition, a large number of spins with very low Kondo temperatures gives a non Fermi-liquid ground state. For this scenario, we find that $\mathrm{Im}\Sigma(\omega) \sim -c + \omega^{1/4}$ at low ω.

$P_{ph}(T_K)$, the distribution of Kondo scales that is relevant to $\mathrm{UCu}_{5-x}\mathrm{Pd}_x$, is intermediate between these two cases.

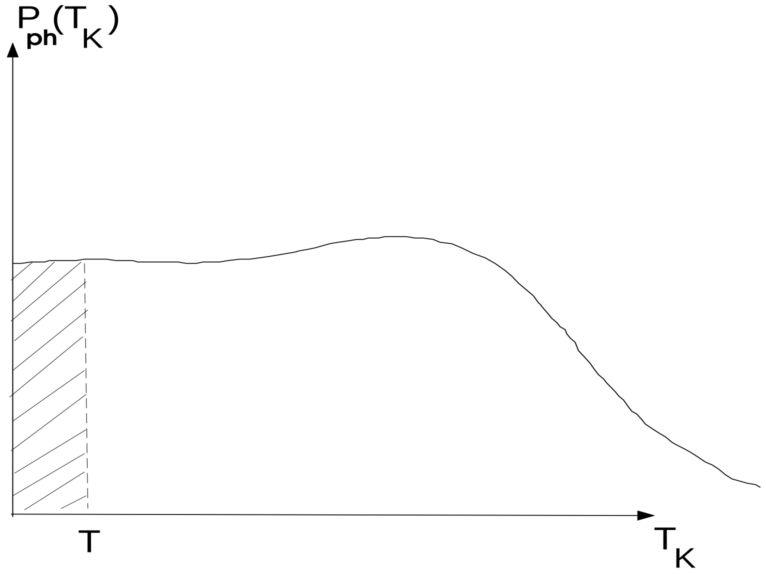

Figure 5.3: *This is the rough shape of the distribution $P_{ph}(T_K)$. At any low temperature T, the main contribution to χ comes from the hatched area, whereas $\rho(T)$ has dominant contributions from $T_K \geq T$*

It gives us an $\mathrm{Im}\Sigma(\omega)$ that behaves like $-c+|\omega|$ as $\omega \rightarrow 0$. This behavior can be understood through the following simple argument. Oliveira's expression for the f-electron spectral function at $T=0$ can be expanded near $\omega=0$ to give a form $A_f(\omega, T_K) \sim 1-\alpha(\omega/T_K)^2$, where α is a constant. Given that $P_{ph}(T_K) \approx constant$ at low T_K, $\int_0^\infty A_f(\omega, T_K)\, P_{ph}(T_K)\, dT_K$ gets its dominant contribution from the region where $T_K \geq \omega$. This would basically be the "unhatched" area of the $P_{ph}(T_K)$ curve in Fig. 5.3. If we change the lower limit of the integral from 0 to ω and make use of the fact that $P_{ph}(T_K)$ has a finite upper cutoff ($\sim 100K$), $\mathrm{Im}\Sigma(\omega)$ turns out to be $-c+|\omega|$. A similar argument was employed by Miranda et al.[20] to calculate the resistivity. Averaging ω over a region of width k_BT near the Fermi surface replaces $|\omega|$ by T, giving a resistivity linear in temperature which is observed experimentally in $Y_{1-x}U_xPd_3$ and $UCu_{3.5}Pd_{1.5}$[8].This result is confirmed by direct calculation of the resistivity (not shown).

Fig. 5.4 shows the temperature dependence of the optical conductivity of the phenomenologically disordered system. Consistent with what is in $Y_{1-x}U_xPd_3$ and $UCu_{3.5}Pd_{1.5}$[10], the Drude-like peak is recovered when $T100K$, since spins with essentially all possible values of T_K are participating in the dynamics at this temperature.

The inset lists the zero temperature optical conductivities for the three distributions of Kondo scales. All are characterized by a vanishing Drude weight at low T, along with a finite frequency peak. As the disorder is increased, this peak moves towards lower frequencies, concomitant with the decrease in the average value of T_K

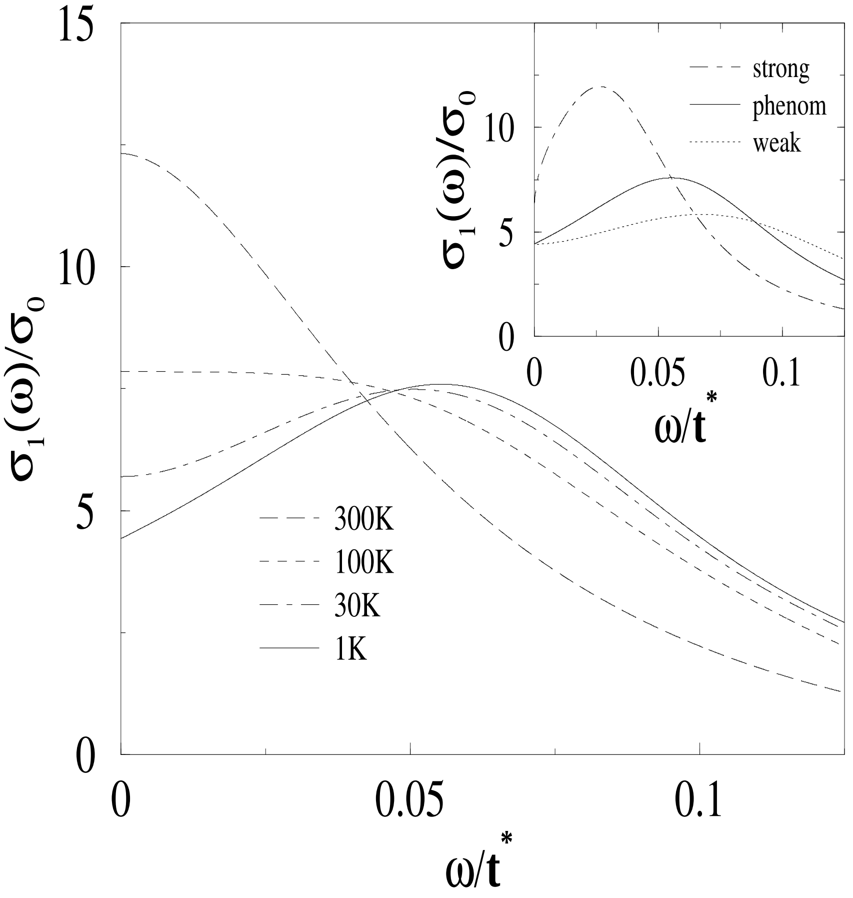

Figure 5.4: *Optical conductivity for the phenomenological distribution of Kondo scales at a few temperatures when $x = 0.2$. At very low temperatures a finite number of unquenched spins preempt the formation of a Fermi-liquid. The interesting feature is the development of a Drude peak as we go from temperatures much below the bulk Kondo value ($T_K^0 \approx 100K$) to those much above it. The inset shows the conductivity for the three different $P(T_K)$ when $T = 0$. The absence of a Drude peak is conspicuous in all three cases.*

(which is different than T_K^0). The Drude peak at $T = 0$ is recovered from the weak disorder case if $u \to 0$ in $P(J)$, giving $P_{wd}(T_K) \propto \delta(T_K - T_K^0)$ (T_K^0 is the bulk value), which takes us to the single Kondo scale physics. The identical $T = 0$ dc value of the conductivity in all three cases is a consequence of the Friedel sum rule at the Fermi level and is an artifact of our framework (we are always in the unitarity limit). $\sigma(\omega = 0, T = 0)$ would be different if the values of x are chosen to be different in the three cases.

The optical conductivity of metals, even non Fermi liquid metals, is usually analyzed by rewriting it in a generalized Drude form [10]

$$\sigma(\omega) = \frac{\omega_p^2}{4\pi} \frac{1}{\Gamma(\omega) - i\omega(1 + \lambda(\omega))}, \tag{5.9}$$

where $\sigma(\omega) = \sigma_1(\omega) + i\sigma_2(\omega)$. We calculate the transport relaxation rate $\Gamma(\omega)$ and the optical mass enhancement $(1 + \lambda(\omega))$ for the three distributions of Kondo scales. However, as shown in Fig. 5.5(a), only the phenomenological distribution results in a linear in frequency zero temperature $\Gamma(\omega)$, consistent with what is seen in $Y_{1-x}U_xPd_3$ and $UCu_{3.5}Pd_{1.5}$[10]. In each case, we find that the low frequency optical mass enhancement $1 + \lambda(0)$ is also negative (however, in the case of weak disorder a positive mass is recovered as $u \to 0$).

$\Gamma(\omega)$ for the phenomenological distribution at several different temperatures is plotted in Fig. 5.5(b). Here, consistent with Degiorgi, et al.[10] we fit the relaxation rate to $\Gamma(\omega) = \Gamma_0\left(1 - (T/T_0)^n - (\omega/\omega_0)^n\right)$ in the low frequency region. We find that $T_0 \approx 85K$ and $\omega_0 \approx 0.09t^*$, and are roughly constant in temperature. At

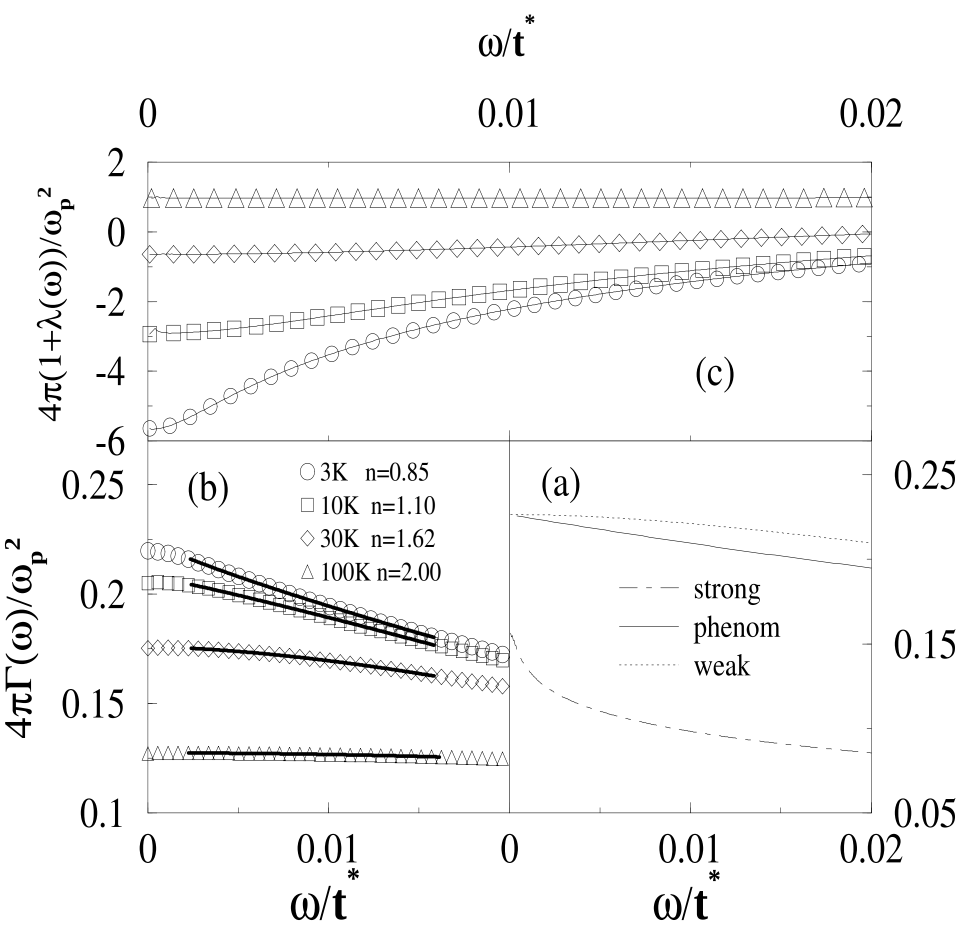

Figure 5.5: *(a) Frequency dependence of the scattering relaxation rate* $\Gamma(\omega)$ *at* $T = 0$ *for the three different* $P(T_K)$ *when* $x = 0.2$. *Note that* $\Gamma(\omega)$ *is linear in* ω, *and therefore consistent with experiment[10], only for the phenomenological distribution of Kondo scales.* $\Gamma(\omega)$ *corresponding to weak disorder has an* ω^2 *behavior as* $\omega \to 0$, *suggesting the formation of a local Fermi liquid. (b)* $\Gamma(\omega)$ *for* $P_{ph}(T_K)$ *at different temperatures; in each case the solid line is a fit to the form* $\Gamma(\omega) = \Gamma_0\,(1 - (T/T_0)^n - (\omega/\omega_0)^n)$. *We see that up until* $10K$, *we have a scattering rate that is roughly linearly decreasing in* ω *and* T. *(c) Optical mass enhancement for* $P_{ph}(T_K)$ *at different temperatures (symbols are the same as (b)). At low temperatures* $1 + \lambda(0) < 0$ *indicative of a non-Fermi liquid.*

high temperatures, $\Gamma(\omega)$ and $1+\lambda(\omega)$ (Fig. 5.5(c)) are weakly frequency dependent, $1+\lambda(\omega) > 0$ and $n = 2.00$, as expected for a Fermi liquid. Thus, as seen in Fig. 5.4, a Drude peak is recovered in $\sigma_1(\omega)$. As the temperature is lowered, $\Gamma(\omega)$ and $1+\lambda(\omega)$ become strongly frequency dependent, $1+\lambda(0) < 0$, and $n \approx 1$, features which we believe should be viewed as characteristic of a non-Fermi liquid. A very similar sequence of features are seen in $Y_{1-x}U_xPd_3$ and $UCu_{3.5}Pd_{1.5}$[10].

5.4 Conclusion.

Within the Kondo disorder model[14, 15, 20], we calculate dynamics for *dilute* U-based heavy Fermion systems. As mentioned in the introduction, this calculation is very well justified for a system with dilute Kondo scatterers ($Y_{1-x}U_xPd_3$) at all temperatures. For a concentrated Kondo lattice system like $UCu_{3.5}Pd_{1.5}$, only the leading temperature(ω) dependence applies (not the numerical prefactor). When temperature(ω) becomes comparable to T_K^0, self-consistent modifications to $P(T_K)$ presumably are significant for the lattice.

We observe a linear resistivity at low T consistent with Ref. [8], the lack of a Drude peak and a low-frequency pseudogap in the real part of the optical conductivity, a negative low temperature optical mass, and a linear in frequency optical dynamical scattering rate. All these features are observed in $Y_{1-x}U_xPd_3$ and $UCu_{3.5}Pd_{1.5}$[8, 10]. It is also straight- forward to compute the spin-relaxation rate in NMR ($1/T_1$), which will be addressed in an upcoming publication. Thus, we conclude that the phenomenological distribution of Kondo scales model is sufficient to describe the dynamics of these disordered systems. It is important to stress that Kondo disorder is not the sole possible explanation of non Fermi-liquid behavior in these systems [12, 13]. In fact, it has recently been shown that the two-channel Kondo lattice model displays remarkably similar optical properties[29]. However, it remains to be seen if an appropriate two-channel Kondo model can accurately describe the transport and optical properties of *dilute* systems such as $Y_{1-x}U_xPd_3$.

Chapter 6

Weak magnetoresistance of disordered heavy fermion systems

Ref: A. Chattopadhyay, M. Jarrell, H. R. Krishna-murthy, H. K. Ng, J. Sarrao and Z. Fisk, *Weak magnetoresistance of disordered heavy fermion systems*, **cond-mat/9805127**

6.1 Introduction

In this chapter we discuss the properties of the disordered Kondo model in a magnetic field, and try to understand the interplay of field and temperature within this scenario. The experimental systems we focus on for comparison are (as in the previous chapter) the U-based compounds $Y_{1-x}U_xPd_3$ and $UCu_{3.5}Pd_{1.5}$ [8, 16] where there is some consensus that the non-Fermi liquid ground states are disorder induced. In a magnetic field both of these systems display a very weak negative magnetoresistance, but a large change in susceptibility [16, 15]. This is in sharp contrast to canonical dilute magnetic alloys with a single small Kondo scale ($La_{1-x}Ce_xB_6$; $T_K \approx 1K$) where one usually sees a strong negative magnetoresistance ($\Delta\rho(H)/\rho(0) \approx 90\%$ at fields $\sim 2-3T$) with a comparable change in the thermodynamic response. We address these two issues in this chapter. First, we discuss the calculation of magnetoresistance within the disordered Kondo model, compare the theoretical results with new experimental data and present a qualitative argument for the observed weak field dependence of $\rho(H)$ at finite temperatures. Second, we present an explanation for the difference in the field dependence of transport and thermodynamic quantities at $T = 0$.

6.2 Formalism

6.2.1 Extension of the Doniach-Sunjic form

The theoretical calculations reported in this chapter use an extension to finite magnetic fields of the formalism developed in the previous chapter [31], where the optical conductivity for a *dilute* collection of Kondo impurities in a disordered host, such as in $Y_{1-x}U_xPd_3$, was calculated assuming a distribution of Kondo temperatures. However, we believe that the leading dependence (at T, H much smaller than the bulk T_K^0) should apply to concentrated systems like $UCu_{3.5}Pd_{1.5}$ as well.

The dilute system may be modelled in terms of symmetric nondegenerate Anderson impurities. In the absence of a magnetic field, the impurity f-density of states has a sharp resonance at the Fermi level, giving significant impurity contributions to the transport, specific heat and magnetic susceptibility. Most of the heavy fermion systems we consider exhibit strong $L - S$ coupling. Hence the dominant effect of the B-field is to Zeeman couple to the f-spins. For a given T_K, the magnetic field splits the up and down f-spins, giving rise to a different spectral function for each spin species. Concentrating on the Kondo limit of the Anderson model ($n_f \approx 1$), the phenomenological expression [31, 25, 4] for the Kondo resonance can be extended to include the magnetic field effects as

$$A_{f\uparrow}(\omega) = \frac{1}{\pi\Delta}\mathrm{Re}\left[\frac{i\Gamma_K}{(\omega - \alpha H + i\sqrt{\Gamma_K^2 + \beta^2 + \gamma^2})}\right]^{1/2} . \tag{6.1}$$

Here α and β are assumed to be functions of magnetic field but independent of temperature, $\Gamma_K = (\pi/2)^2 T_K$, Δ is the f-d hybridization energy and $\gamma(T/T_K)$ is a universal function that captures the temperature dependence of the spectrum [31]. The Zeeman-like term α reflects the shift in the spectral peak with respect to the Fermi energy. Particle-hole symmetry implies that $A_{f,\uparrow}(\omega) = A_{f,\downarrow}(-\omega)$.

At $T = 0$, the impurity magnetization is given by (in units of $\frac{g\mu_B}{2}$)

$$m(H/T_K) = \int_{-\infty}^{0} d\omega \left[A_{f\uparrow}(\omega, H/T_K) - A_{f\downarrow}(\omega, H/T_K)\right] . \tag{6.2}$$

When $H/T_K << 1$, it is reasonable to assume that to leading order $\alpha(\frac{H}{T_K}) \approx \alpha_0$ and $\beta(\frac{H}{T_K}) \approx \beta_0 \frac{H^2}{T_K^2}$ (where the prefactors α_0 and β_0 are now constants). Under these assumptions, when eq.(2) is expanded upto $O(\frac{H}{T_K})^3$, we have

$$m(H/T_K) \approx \frac{4T_K}{\pi\Delta}\left[\frac{\alpha_0}{2}(\frac{H}{T_K}) - (\frac{\alpha_0^3}{16} + \frac{\alpha_0\beta_0}{8})(\frac{H}{T_K})^3\right] . \tag{6.3}$$

By comparing the right hand side of eq.(3) to the Bethe ansatz expression for the low-field impurity magnetization in powers of $\frac{H}{T_K}$ [32] we get the low H values of α, β.

In principle the Bethe ansatz series (which is valid for $H \leq T_K$) can be reproduced only by using an infinite number of coefficients in our spectral function, but α_0 and β_0 capture the dominant low field effects. This is confirmed at a low $T \neq 0$ by calculating the f-spectra of the symmetric Anderson model in a finite field by Quantum Monte Carlo(QMC). The numerical analytic continuation is done using maximum entropy method (MEM) [21, 22], with the perturbation theory spectrum as the high temperature default. Using the MEM results, the expression for the spectral function can be calibrated and $\alpha(H/T_K)$ and $\beta(H/T_K)$ determined over a wide range of field values. The results are shown in Fig. 6.1. The fits tend to be reasonable until the frequency reaches the charge transfer peak.

6.3 Results

Fig. 6.2a and Fig. 6.6b show some new experimental data for the magnetoresistance of $UCu_{3.5}Pd_{1.5}$ and Figs. 2b and 3a the calculated values. The experimental measurements were made on a polycrystalline sample of size 3.0 mm by 0.47 mm by 0.52 mm. The sample was grown by arc melting the constituents and sealed in quartz tube and annealed for 10 days at 800^{o}C. The resistivity was measured using a 4 probe technique in a 12 Tesla Oxford superconducting magnet. A constant current of 10 mA was used for all the measurements. To eliminate the possibility of any heating effect, the current was reduced to 5 mA for one of the temperature scans. No discernible

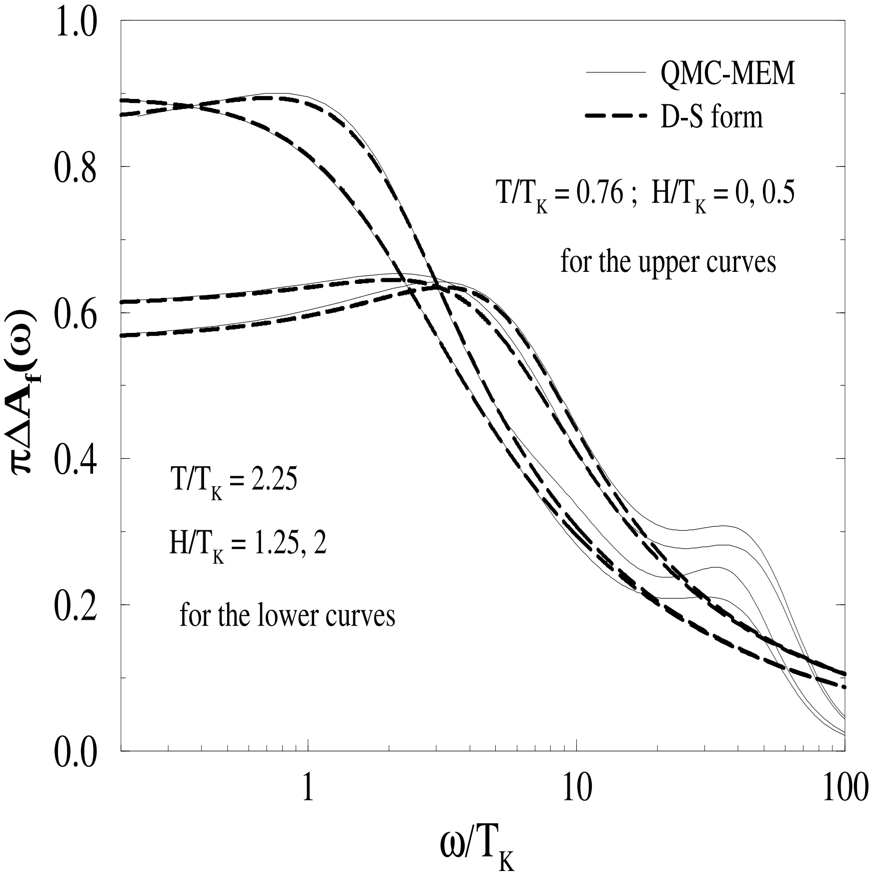

Figure 6.1: *Spectral function for the up-spin f-electron in the Kondo limit of the Anderson model for different* T/T_K *and* H/T_K *values. The dashed lines are the result of the extended Doniach-Sunjic function. The solid lines are the QMC/MEM results. The fit is very reasonable until the charge transfer physics becomes important.*

difference was observed. The calculations were done assuming $T_K^0 = 100K$ which is roughly the bulk Kondo temperature in $UCu_{3.5}Pd_{1.5}$.

As one can see, there is strong qualitative resemblance between the experimental and theoretical curves. The general trend is that at very low T, there is a negative magnetoresistance even at the lowest fields. As one increases T, $\rho(H)$ is relatively constant upto field values comparable to the temperature, beyond which there is a downturn. From Fig. 2, we see that there is almost quantitative agreement at $4K$. At $20K$, we are at temperatures comparable to T_K^0 and the self-consistent modifications to $P(T_K)$ presuambly are significant for the lattice. The qualitative agreement is still there in that $\rho(H, T = 20K)$ is nearly a constant over $12T$.

This interplay of magnetic field and temperature can be understood as follows. Let us look at the temperature dependence of the susceptibility and resistivity for a given Kondo scale. In the case of $\chi(T/T_K)$, the $T = 0$ value is given by $\frac{1}{T_K}$, which means that lowering the Kondo temperature will result in an enhancement of $\chi(T = 0)$. A similar argument holds for C_V/T as well. So in a system with a distribution of Kondo scales, the low T thermodynamics (χ, C_V) are dominated by the sites with the lowest T_K values (Fig. 6.3).

The case of resistivity is different since for any fixed T_K, $\rho(T = 0)$ is pinned at the unitarity limit. Hence lowering of the Kondo scales will end up "squeezing" the "local Fermi liquid" regime in temperature (where $\delta\rho(T/T_K)$ scales like $1 - (T/T_K)^2$).

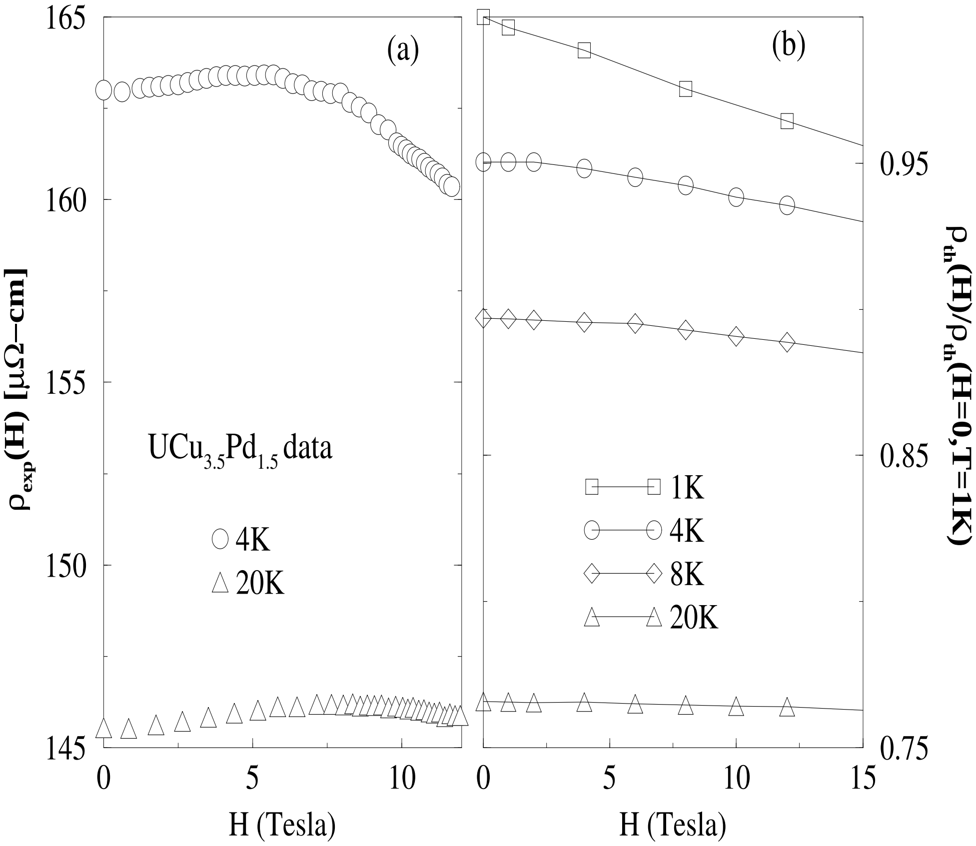

Figure 6.2: *Magnetic field dependence of the resistivity. Both the experimental measurements (a) on $UCu_{3.5}Pd_{1.5}$ and theoretical plots (b) are shown. The qualitative agreement is quite reasonable. The magnetoresistance becomes negative at field values comparable to the temperature. This is because transport at a given T is dominated by sites that have $T_K \approx T$ or higher. As a result, at any given T the resistivity is unaware of the field until H suppresses the relevant T_K.*

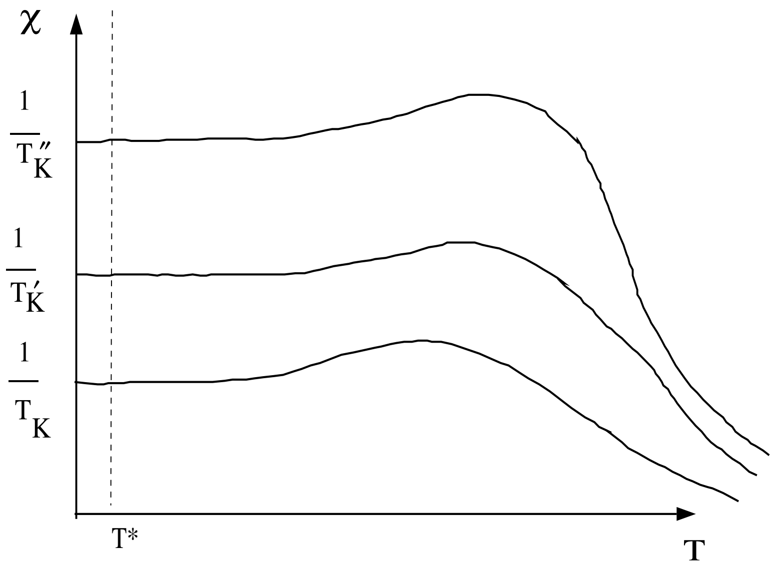

Figure 6.3: *Susceptibility curves for three different Kondo temperatures* $T_K > T_K^{'} > T_K^{''}$. *The main contribution at a low temperature* T^* *comes from the lowest Kondo scales.*

As a result, the dominant (but by no means exclusive) contribution to transport at low T comes from sites with high Kondo scales, particularly $T_K > T$ (Fig. 6.4).

Now, in the presence of a broad distribution $P(T_K)$, consider a temperature T and a field $H << T$ as shown in Fig. 6.5. For any site with $T_K \leq H$ the Kondo singlet will be broken. Since these low T_K sites are the ones dominating the thermodynamics, any finite magnetic field will have an appreciable effect on χ. On the other hand, a majority of the sites that affect transport at T are unaware of this low field. The field dependence of the resistivity shows up only when $H \approx T$, where the system acquires an increasing number of free spins by breaking the relevant Kondo singlets. This gives rise to a weak negative magnetoresistance which is confirmed by the magnetotransport

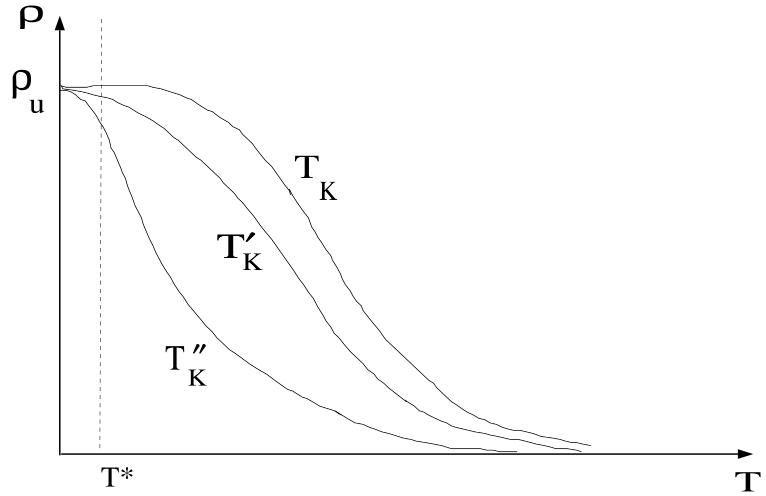

Figure 6.4: *Resistivity curves for three different Kondo temperatures* $T_K > T_K^{'} > T_K^{''}$. *Contrary to* $\chi(T)$, *the main contribution at a low temperature* T^* *comes from the highest Kondo scales. Since many of the sites scatter close to the unitarity limit, the entire distribution becomes important for transport.*

measurements on $UCu_{3.5}Pd_{1.5}$. The broadness of $P(T_K)$ in this case is crucial for $\Delta\rho(H)/\rho(0)$ to be weak compared to $La_{1-x}Ce_xB_6$, for instance. This is because even when $H \approx T$, there are a significant number of sites that have Kondo scales $T_K >> T, H$ that contribute to the resistivity through nearly unitary scattering.

A natural extension of this argument would suggest a gentle initial upturn in the resistivity data at $H \approx T$ if there is an initial upturn in $P(T_K)$. This trend is noticed in the data on $UCu_{3.5}Pd_{1.5}$ [Fig. 5.2(a),5.6(b)], indicating that the distribution of Kondo scales in the real sample is not really flat at the low T_K end but has an

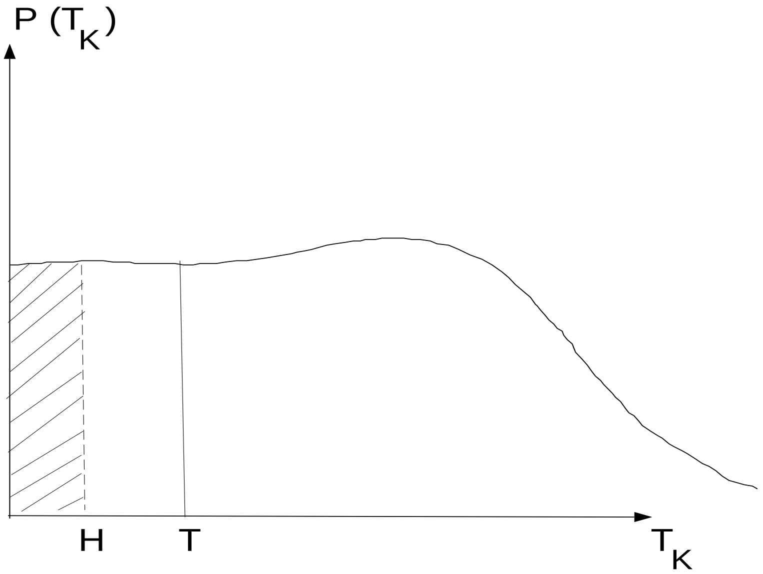

Figure 6.5: *Interplay of H and T in the presence of a distribution $P(T_K)$. For a low temperature T and a given field H, the Kondo effect is killed for sites with $T_K \leq H$ (the hatched area in the figure). These are the spins important for $\chi(T)$ but not so much for $\rho(T)$.*

upward slope. We have calculated $\rho(H,T)$ for such a distribution and confirmed this behaviour.

We have also re-calculated χ within our framework (earlier calculations were done by Bernal et al. [15] and Miranda et al. [20]) to illustrate the difference with resistivity in a field and show the results in Fig. 6.6(c). Here, for consistency with experiments, $\chi(T)$ is defined as $\overline{m(H,T)}/H$ where $\overline{...}$ denotes disorder averaging. The resistivity responds to the magnetic field much more weakly than χ does. At $T = 1K$, ρ changes by 3% when a 6 Tesla field is applied to the system; χ changes by 24% over the same range. This is in qualitative agreement with the experiments on $Y_{1-x}U_xPd_3$ and $UCu_{3.5}Pd_{1.5}$.

The significantly different field dependence of ρ and χ can be understood as follows from the $T = 0$ Bethe ansatz expression relating the magnetization to the resistivity in the single impurity Kondo model:

$$R_{imp}(H/T_K) = R_{imp}(0)\cos^2\left[\frac{\pi}{2}f(x)\right]. \qquad (6.4)$$

Here $x \equiv \frac{g\mu_B H}{k_B T_K} = \frac{\tilde{H}}{T_K}$ and $f(x) = \frac{2}{g\mu_B}m(x)$. Disorder averaging, for simplicity, over a rectangular distribution of T_K upto T_K^0, one gets

$$\frac{\overline{R_{imp}(H)}}{R_{imp}(0)} \sim \frac{\tilde{H}}{T_K^0}\int_{\frac{\tilde{H}}{T_K^0}}^{\infty}\cos^2\left[\frac{\pi}{2}f(x)\right]\frac{1}{x^2}dx \qquad (6.5)$$

$$\overline{\chi_{imp}(H)} \sim \int_{\frac{\tilde{H}}{T_K^0}}^{\infty} f'(x)\frac{1}{x}dx\,. \qquad (6.6)$$

For large $\tilde{H}$, the integrals are dominated by large x where the integrands scale like $\frac{\pi^2}{16}\frac{1}{(x\ln(x))^2}$ and $\frac{1}{2}\frac{1}{(x\ln(x))^2}$ respectively. So the integrals are comparable for large $\frac{\tilde{H}}{T_K^0}$, implying that $\overline{\chi_{imp}}$ falls off faster than $\overline{R_{imp}(H)}$. For small $\frac{\tilde{H}}{T_K^0}$, $\overline{\chi_{imp}}$ has a log divergence from the small x region. The resistivity integral has a $\frac{T_K^0}{\tilde{H}}$ divergence as well, but it gets balanced out by the prefactor. Hence, $\overline{R_{imp}(H)}$ has a weaker dependence on field compared to $\overline{\chi_{imp}(H)}$ for both large and small values of $\frac{\tilde{H}}{T_K^0}$.

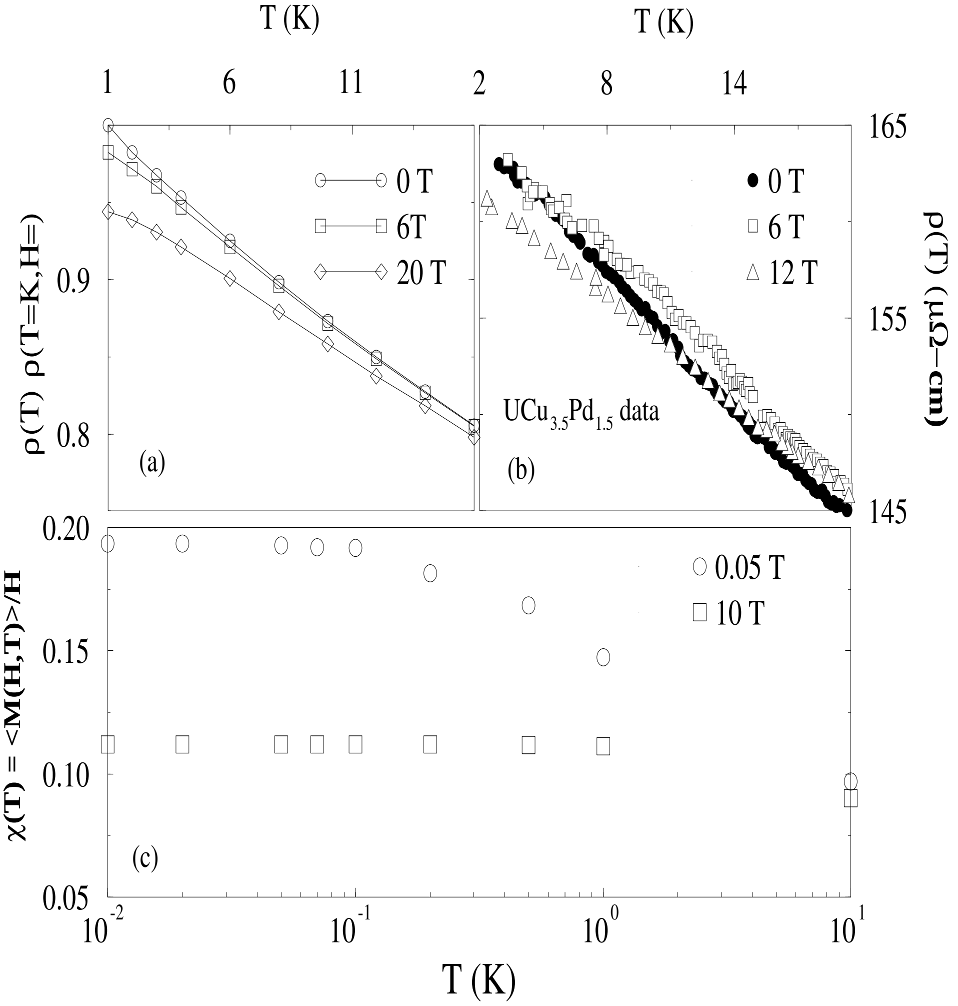

Figure 6.6: *Resistivity and impurity spin susceptibility within the disordered Kondo model. The susceptibility shown is normalized with its value at* $0.01K, 0.05$ *Tesla. One notices a far more pronounced effect of magnetic field on* $\chi(T)$ *at low temperatures, compared to* $\rho(T)$*. For instance, at* $T = 1K$*,* ρ *is estimated to change by* 3% *over* $6T$*;* χ *changes by* 24% *over the same field value.*

6.4 Conclusion

We have presented calculations of magnetoresistance within the disordered Kondo scenario and new experimental data for the magnetoresistance in $UCu_{3.5}Pd_{1.5}$ at a variety of temperatures and find the results to be consistent. The weak magnetoresistance of this system at finite temperature has been qualitatively explained by examining the interplay of field and temperature in the presence of a wide distribution of Kondo scales. Finally, we have addressed the stronger field dependence of susceptibility as compared to transport and presented a calculation at $T = 0$ to explain this.

Chapter 7

Non Fermi Liquid Dynamics of the Two-Channel Kondo Lattice

Ref: M. Jarrell, Hanbin Pang, D. L. Cox, F. Anders and A. Chattopadhyay, *Non-Fermi-liquid dynamics of the two-channel Kondo lattice*, Physica B, **230-232**,557(1997)

7.1 Introduction

In this chapter, we present the first rigorous solution for the dynamics of the two-channel Kondo lattice model in infinite spatial dimensions. We find that the paramagnetic phase of this model is an "incoherent metal" with finite density of states at the Fermi energy and finite residual resistivity. Both the single-particle and the optical excitations are non-Fermi liquid like; in particular, there is a finite lifetime for electrons at the Fermi energy, an ill defined quasiparticle mass, a linear low temperature electrical resistivity with a finite residual value, a negative optical mass and a linear in frequency low temperature scattering relaxation rate.

7.2 Motivation and Model

The two-channel Kondo impurity model consists of two identical species of non-interacting electrons antiferromagnetically coupled to a spin 1/2 impurity. It is energetically favourable for both the conduction bands (denoted by 1 and 2 in Fig. 7.1) to couple to the impurity (the central spin in the figure).

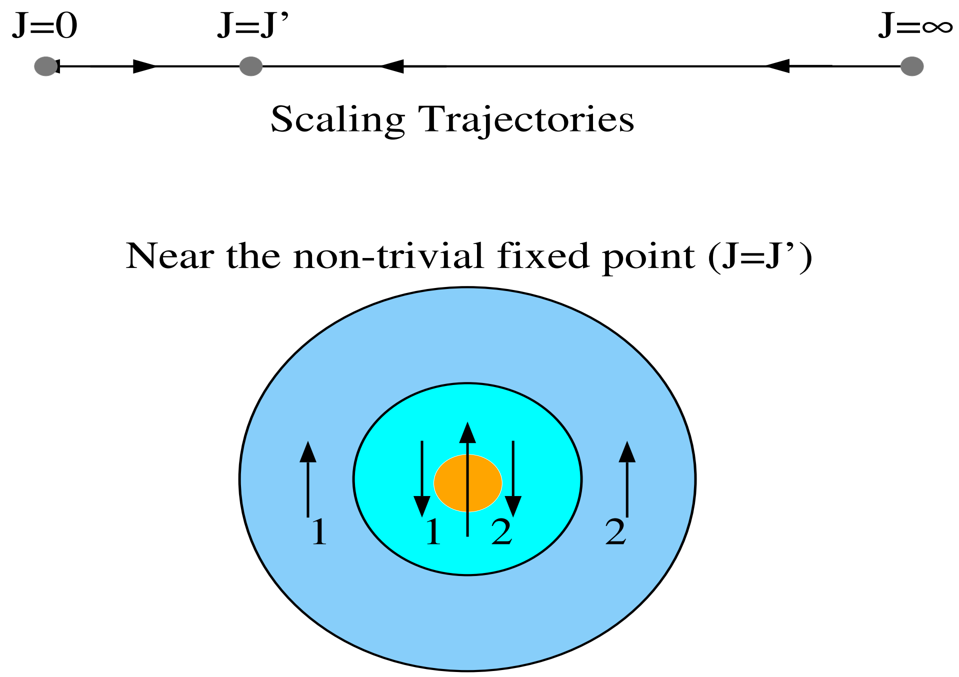

Figure 7.1: *Inability of the two conduction bands to screen the impurity at any low T (or large length) scales. J=0 is the free moment; J=∞ is the Fermi-liquid fixed point. This system flows towards a finite J fixed point, which is a non-Fermi liquid.*

Let us start from the smallest length scale (the inner circle $\sim$ one lattice spacing), or equivalently, at a high temperature. The spin-spin interactions will clearly give a spin-1/2 object. If we go to the next length scale (the bigger circle), the two channels of conduction spin (now both up) and the impurity bind to form a new effective spin-1/2 object which serves as an impurity to conduction states outside that length scale. So, even at the largest length scales as the temperature goes to zero, there is always a spin-1/2 complex left over and we have a Non-Fermi liquid. In terms of scaling trajectories, Nozières and Blandin [37] showed that the two-channel Kondo impurity flows towards a finite $J = J'$ fixed point (Fig. 7.1), whereas $J = \infty$ is the Fermi-liquid fixed point.

As a result, the ground state is degenerate and the excitation spectrum non-Fermi liquid like. We believe that at least the qualitative features of the model will change greatly once the concentration of impurites becomes finite. A single impurity always lives in a Fermi liquid host; whereas the introduction of a second impurity to the system will mean that at some temperature, the host of each impurity will be a non Fermi liquid due to the presence of the other. The simplest model to test this hypothesis is the fully concentrated one; ie. the two-channel kondo lattice model.

The Hamiltonian for the two-channel Kondo lattice is

$$H = J\sum_{i,\alpha} \mathbf{S}_i \cdot \mathbf{s}_{i,\alpha} - \frac{t^*}{2\sqrt{d}} \sum_{<ij>,\alpha,\sigma} \left(c^\dagger_{i,\alpha,\sigma} c_{j,\alpha,\sigma} + \text{h.c.} \right) - \mu \sum_{i,\alpha,\sigma} c^\dagger_{i,\alpha,\sigma} c_{i,\alpha,\sigma} \,, \tag{7.1}$$

where $c^\dagger_{i,\alpha,\sigma}$ ($c_{i,\alpha,\sigma}$) creates (destroys) an electron on site i in channel $\alpha = 1, 2$ of spin σ, $\mathbf{S}_i$ is the Kondo spin on site i, and $\mathbf{s}_{i,\alpha}$ are the conduction electron spin operators for site i and channel α. The sites i form an infinite-dimensional hypercubic lattice. Hopping is limited to nearest neighbors with hopping integral $t \equiv t^*/2\sqrt{d}$; the scaled hopping integral t^* determines the energy unit and is set equal to one ($t^* = 1$). Thus, on each site the Kondo spin mediates spin interaction between the two different channels. This problem is non trivial, and for the region of interest in which $J > 0$ and $T \ll J$, t^* it is describable only with non-perturbative approaches. Clearly some simplifying method which allows for a solution of the lattice problem in a non-trivial limit is necessary.

7.3 Formalism and Simulation

Such a method was proposed by Metzner and Vollhardt [17] who observed that the renormalizations due to local two-particle interactions become purely local as the coordination number of the lattice increases. A consequence is that the solution of most standard lattice models may be mapped onto the solution of a local correlated system coupled to an effective bath that is self-consistently determined[39]. We briefly outline this mean-field method in Chap. 4. The above references and some recent reviews provide further details on the method[40]. In order to solve the remaining impurity problem, we use the Kondo impurity algorithm of Fye and Hirsch[19], modified to simulate the two-channel problem[41]. Most of our simulations were limited to the model at half filling of the conduction bands ($N = 1.0$ for $J = 0.75, 0.625, 0.5, 0.4$); however, we have also studied the system away from half filling ($N = 0.75$ and 0.50) for two values of J ($J = 0.75$ and 0.625). A sign problem was also encountered in the QMC process which limited our access to very low temperatures. The Euclidean-time QMC results for the local greens function $G(\tau)$ were then analytically continued to real frequencies using the "annealing" Maximum Entropy method[22]. The single particle self energy may then be obtained by inverting the relation $G(\omega) = -i\sqrt{\pi}w\left(\omega + \mu - \Sigma(\omega)\right)$, where $w(z)$ is the complex Fadeev function. Error bars are ill-defined for individual points in analytically continued spectra[22], and are less than 3% for the other results presented here.

7.4 Results

As the temperature is lowered, the local susceptibilities show evidence of Kondo screening: the screened local Kondo moment $T\chi(T)$ falls like $T\ln(T)$, and the local Kondo spin-conduction spin correlation indicates an antiparallel alignment $\langle \mathbf{S}_i \cdot \mathbf{s}_{i,\alpha} \rangle < 0$; whereas local spin-spin correlation function between the channels indicates a weak parallel alignment $\langle \mathbf{s}_{i,2} \cdot \mathbf{s}_{i,1} \rangle > 0$. By comparing the susceptibility of the local moment to the impurity susceptibility, we are able to estimate the Kondo scale T_0 from the defining relation $T_0\chi(T_0) = 0.3$. We find that $T_0 \simeq 0.85J\exp(-1.01t^*/J)$. For comparison, in the impurity limit we would anticipate $T_0^{imp} \simeq \pi^{-1/2}J\exp(-\sqrt{\pi}t^*/J)$. Hence, T_0 is collectively enhanced in the lattice, as found in the one channel Anderson lattice problem near half filling[50, 51, 52]; we discuss our enhancement further below.

When the temperature is lowered below T_0, we find non-Fermi liquid behavior in the single-particle properties of the model. For example, the derivative of the particle distribution function $dn(\epsilon_k)/d\epsilon_k = -T\sum_n 1/(i\omega_n - \epsilon_k + \mu - \Sigma(i\omega_n))^2$ saturates to a finite width distribution[42], in contrast to a Fermi liquid where it would display a dominant delta function contribution as $T \to 0$, and a Luttinger liquid[35] or Marginal Fermi liquid[43] where it would have a singular divergence.

In Fig. 7.2 we show one electron properties of the model. Fig. 7.2(a) displays the single particle DOS. This has a finite value as $\omega, T \to 0$, with a peak away from the Fermi energy. Note that suppression of $N(\omega = 0)$ leads to an enhanced effective medium DOS which accounts qualitatively for our collectively enhanced T_0 values.

Novel behavior is seen in the real part of the one electron self energy which has positive slope at $\omega \to 0$ (Fig. 7.2(c)). For a Fermi liquid, this slope would be negative. The physical content is important: $Z = 1/(1 - \partial Re\Sigma/\partial\omega)$ measures the overlap of the quasiparticle wave function with the original one-electron wave function having the same quantum labels. A positive slope leads to $Z > 1$ or $Z < 0$, indicating a breakdown of the quasiparticle concept. Concomitant with the finite width of $-dn/d\epsilon_k$ is a finite imaginary part to the low temperature self energy (Fig. 7.2(b)). This indicates that the one-electron excitations are ill defined on approach to the Fermi surface, again ruling out a Fermi liquid description. Since the low temperature thermodynamic properties such as the specific heat, uniform magnetic susceptibility, and charge susceptibility display no evidence for a gap, we believe the observed behavior indicate a new kind of metallic state.

From our numerical results, one can show that the zero temperature self energy must be non-analytic. If the self energy is analytic everywhere on the real axis (and

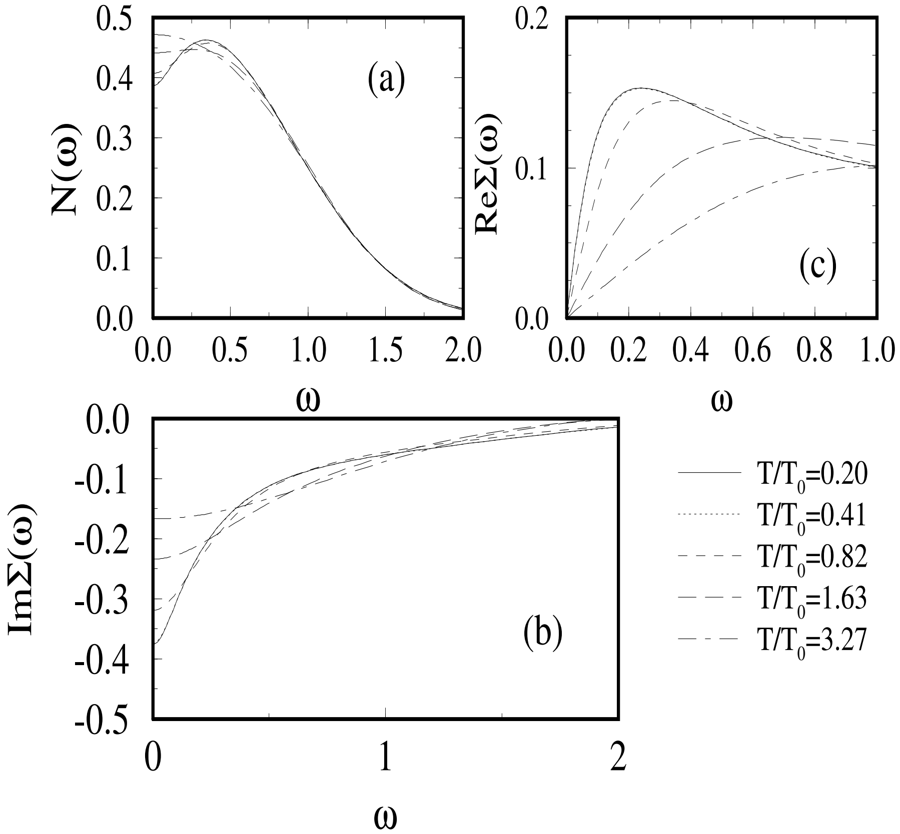

Figure 7.2: *Single particle properties of the two-channel Kondo lattice in infinite dimensions when $J = 0.750$ and $N = 1.0$. (a) Single-particle density of states (DOS). At high temperatures $T \gg T_0$ (not shown), the DOS is a gaussian, crossing over to the peaked distribution with relative suppression at $\omega \to 0$ for lower temperatures when $T \ll T_0$. (b) Imaginary part of the self energy. As the temperature is lowered the self energy does not approach a Fermi liquid form* $\mathrm{Im}\Sigma(\omega) \propto -T^2 - \omega^2$, *but rather appears to approach the non-analytic form (see text)* $\mathrm{Im}\Sigma(\omega) \propto -c + |\omega|$. *(c) The real part of the self energy* $\mathrm{Re}\Sigma(\omega)$, *is also anomalous since its initial slope is positive indicating a quasiparticle renormalization factor which is greater than one.*

the upper half complex plane), then one may easily show that

$$\lim_{T\to 0}\frac{\mathrm{Im}\Sigma(i\omega_0)}{\omega_0}=\lim_{T\to 0}\left.\frac{d\mathrm{Re}\Sigma(\omega)}{d\omega}\right|_{\omega=0}, \tag{7.2}$$

where $\omega_0 = \pi T$ is the lowest Fermionic Matsubara frequency along the imaginary axis. However, we find that when $T < T_0$, $\frac{\mathrm{Im}\Sigma(\omega_0)}{\omega_0} < 0$ and is apparently divergent; whereas, from Fig. 2 it is apparent that $\left.\frac{d\mathrm{Re}\Sigma(\omega)}{d\omega}\right|_{\omega=0} \approx 1$. Thus, $\Sigma(\omega)$ cannot be analytic at the origin of the complex plane.

The non-Fermi liquid behavior also strongly effects experimentally relevant transport properties of the system. The electrical resistivity is shown in Fig. 7.3.

We find that $\rho(T)/\rho(0)$ curves for different J values collapse onto a universal scaling curve when plotted against T/T_0. As shown in the inset, $\rho(T) \simeq \rho(0)[1+B(T/T_0)]$ for $T \to 0$, with $B < 0$[?]. We interpret the finite value of $\rho(0)$ together with $-Im\Sigma(0,0)$ as "spin disorder scattering" off of the degenerate screening clouds centered about each local moment spin. Given the finite density of one particle excitations at the Fermi energy, this finite residual resistivity is indicative of an "incoherent metal phase" brought about by the disordered spin degrees of freedom, in qualitative agreement with results obtained with a Lorentzian bare conduction DOS (which doesn't self-consistently renormalize)[44]. We conjecture that the antiferromagnetism at half filling will lift the disorder at each site and produce an insulating state due to the cell doubling.

As shown in Fig. 5.4, consistent with the lack of quasiparticles, the optical conductivity displays vanishing Drude weight at low temperature. To confirm this, we

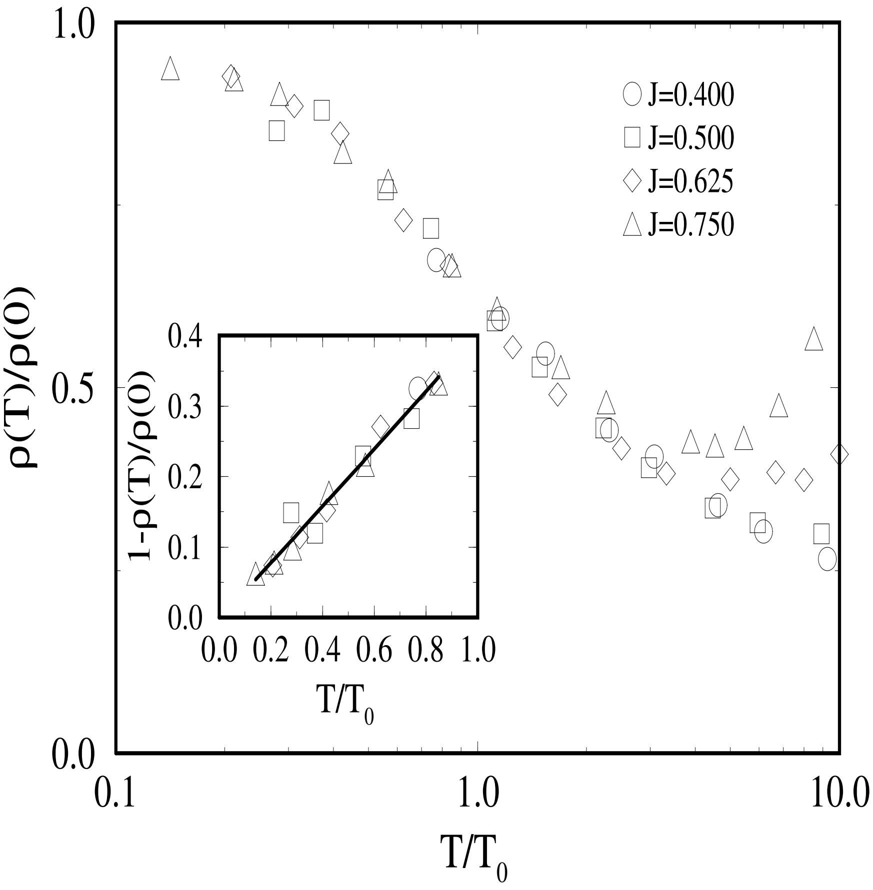

Figure 7.3: *Resistivity of the two-channel Kondo lattice.* $\rho(T)/\rho(0)$ *is plotted versus* T/T_0 *for various values of* J*. In the inset, the lowest temperature data (for* $T/T_0 < 1$*, shown as open circles) was fit to* $\rho(T)/\rho(0) = 1 + B\,(T/T_0)^{\alpha}$*, with* $B = -0.4$ *and* $\alpha = 1.03$.

also calculated the Drude weight, D, by extrapolation[45], $D \propto \chi_{jj}(q = 0, i\omega_n \to 0) - \chi_{jj}(q = 0, i\omega_n = 0)$, where $\chi_{jj}(q = 0, i\omega_n)$ is the bulk current-current susceptibility. For each value of J and all fillings, we found that the extrapolated zero-temperature Drude weight was zero. In addition, there is a finite-frequency ($\omega \approx J$) peak. Both these features again support our interpretation in terms of a new kind of non-Fermi liquid metallic state.

The optical conductivity of metals, even non-Fermi liquid metals, is usually analyzed by rewriting it in a generalized Drude form[10]

$$\sigma(\omega) = \frac{\omega_p^2}{4\pi} \frac{1}{\Gamma(\omega) - i\omega m^*(\omega)} . \tag{7.3}$$

where $\sigma(\omega) = \sigma_1(\omega) + i\sigma_2(\omega)$. Given the nonanalytic nature of the self energy, and thus, presumably the dynamic current-current susceptibility, it is important to calculate $\sigma_2(\omega)$ exactly the same way that the experimentalist do, using a Hilbert transform of $\sigma_1(\omega)$ (rather than the dynamic current-current susceptibility, $-i\omega\sigma(\omega)$.)

The resulting mass enhancement and scattering relaxation rate $\Gamma(\omega)$ are shown in Fig. 7.5(a) when $J = 0.625$ for various temperatures. The lifetime approximation becomes exact in infinite dimensions. Here, for a fermi liquid, one expects $m^*(\omega) = 1 - \frac{2}{\omega}\mathrm{Re}\Sigma(\omega/2)$ and $\Gamma(\omega) = -2\mathrm{Im}\Sigma(\omega/2)$. At high temperatures, $\Gamma(\omega)$ is essentially flat; whereas as T is lowered it appears to develop a significant frequency dependence. Its behavior is quite reminiscent of the imaginary part of the self energy, indicating that the optical and quasiparticle scattering rates are consistent for this model, even though quasiparticles do not exist. The mass enhancement is plotted in Fig. 7.5(b)

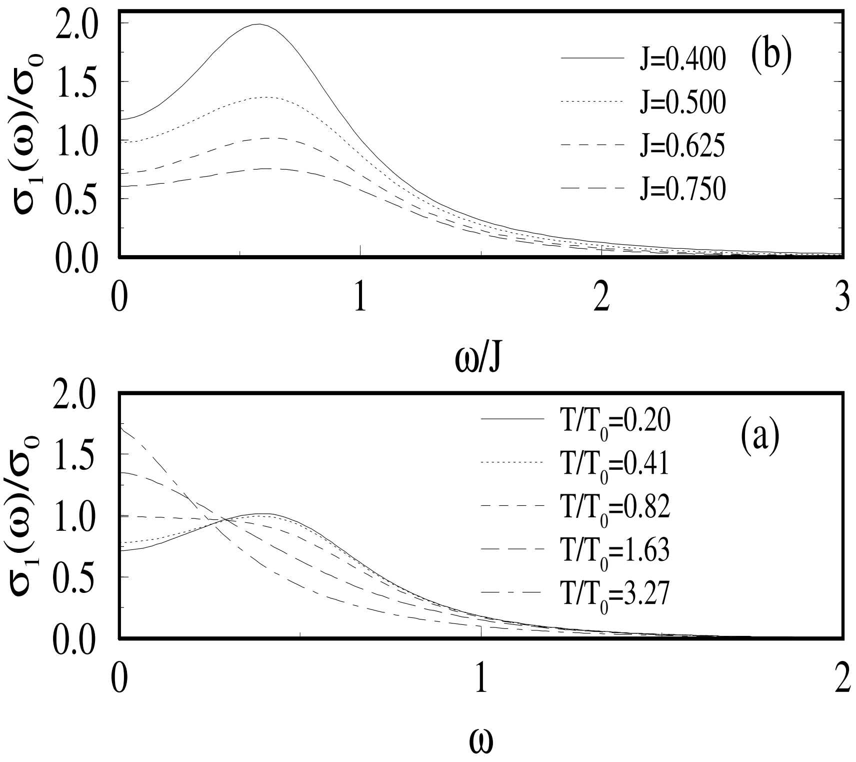

Figure 7.4: *Optical conductivity of the two-channel Kondo lattice. (a) Optical conductivity when* $J = 0.625$. *As the temperature is lowered* $T < T_0$, *the optical conductivity developes a pseudogap at low frequencies. No evidence of a finite Drude weight, D, can be seen, consistent with estimates of D obtained from extrapolation of matsubara-frequency results[45]. (b) The optical conductivity vs.* ω/J *when* $T = 0.0156$ *for various values of J.* $\sigma(\omega)$ *displays a finite-frequency peak at roughly* $\omega \approx 0.6J$.

5.4

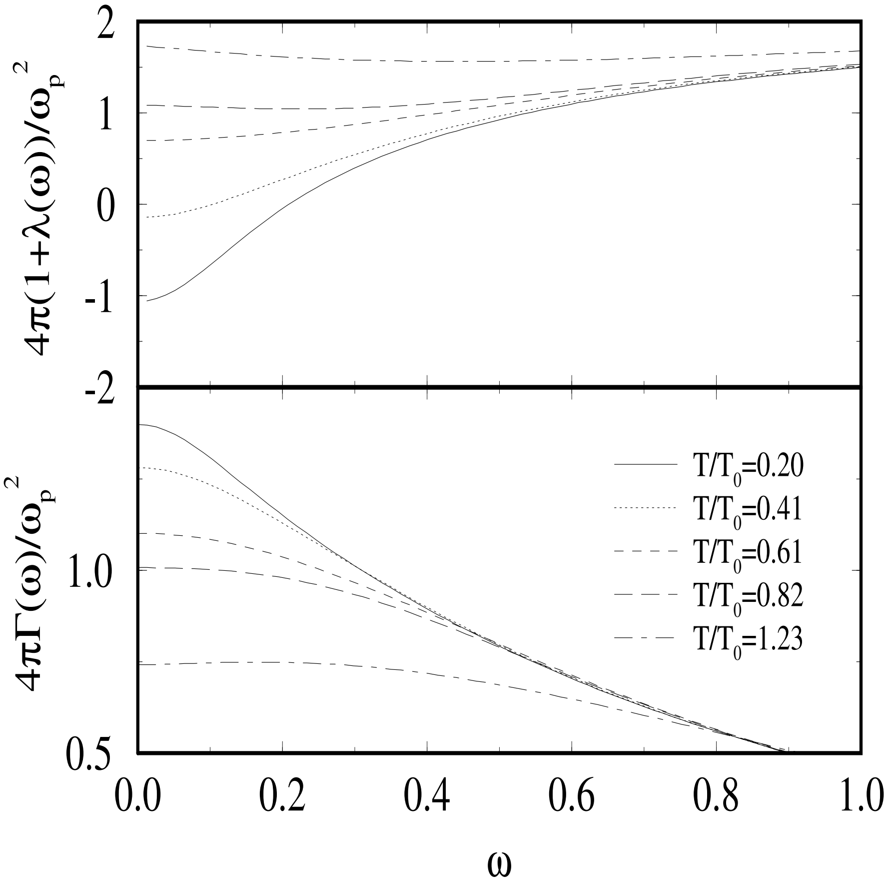

Figure 7.5: *Optical scattering rate* $\Gamma(\omega)$ *(a) and mass enhancement* $m^*(\omega)$ *(b) obtained from the optical conductivity shown in Fig. 5.4(a) using Eq. 7.3. For* $T/T_0 \ll 1$ *both* $\Gamma(\omega)$ *and* $m^*(\omega)$ *display non fermi liquid behavior:* $\Gamma(\omega)$ *is roughly linear in* ω *and* $m^*(0) < 0$. *Typical Fermi liquid behavior is recovered when* $T/T_0 1$, *since both* $\Gamma(\omega)$ *and* $m^*(\omega)$ *become weakly frequency dependent consistent with the recovery of the Drude peak in Fig. 5.4(a).*

for the same parameters. Note that when $T/T_0 < 1$, the low frequency optical mass is negative. This behavior is only qualitatively consistent with the mass estimated from the self energy, since at these temperatures the quasiparticle mass enhancement $1 - d\mathrm{Re}\Sigma(\omega)/d\omega|_{\omega=0} \approx 0$ (cf. Fig. 7.2). The negative mass enhancement should be view as a characteristic feature of a non Fermi Liquid, and the disparity between the two estimates of the mass enhancement provides further evidence that the quasiparticle concept breaks down in this model.

Finally, we mention the possible applicability of our results to concentrated heavy Fermion systems. Three systems display resistivity of the form $\rho(T) \approx \rho(0)[1 + B(T/T_0)^\alpha]$ for $T < T_0$, with $\rho(0)$ of order the unitarity limit and $\alpha \approx 1$. They are: $UCu_{5-x}Pd_x$ (with $B < 0$)[8], UBe_{13} ($B > 0$)[33, 47, 48], and $CeCu_2Si_2$ ($B > 0$)[34]. UBe_{13} and $CeCu_2Si_2$ are ordered compounds which have been proposed as possible two-channel lattice systems (see Refs.[37](b,c)); however, to our knowledge there are no published results for the optical conductivity of these materials. While $UCu_{5-x}Pd_x$ is a possible example of the distribution of Kondo scales scenario[14], it's $\sigma_1(\omega)$ and $\Gamma(\omega)$ are strikingly similar to those diplayed in Figs. 5.4 and 7.5[10] as shown in Fig. 3.6. We have not yet found a conclusive way to differentiate these two mechanisms, just from their response functions.

Bibliography

[1] P. W. Anderson, Basic notions of Condensed Matter Physics, Addison-Wesley (1997).

[2] J. W. Negele and Henri Orland, Quantum Many-Particle Systems, Addison-Wesley (1988).

[3] K. G. Wilson, Rev. Mod. Phys. **56**, 755 (1975).

[4] H.R Krishna-murthy, J.W. Wilkins and K.G. Wilson, Phys. Rev. B **21**, 1003 (1980); **21**, 1044 (1980).

[5] J. R. Schrieffer, P. A. Wolff, Phys. Rev. **149**, 491 (1966).

[6] K. Samwer and K. Winzer, Z. Physik B **25**, 269 (1976).

[7] Kei Yosida, Theory of magnetism, Springer (1991).

[8] For a recent review, see M.B. Maple *et al.*, J. Low Temp. Phys. **99**, 223 (1995), and references cited therein.

[9] M. B. Maple *et al.*, J.Phys. :Cond. Matter **8**, 9773 (1996)

[10] L. Degiorgi, H.R. Ott, and F. Hulliger, Phys. Rev. B **52**, 42 (1995); L. Degiorgi and H.R Ott, J.Phys. :Cond. Matter **8**, 9901(1996); and L.Degiorgi *et al.*, Phys. Rev. B **54**, 6065 (1996).

[11] H. v. Löhneysen *et al.*, Phys. Rev. Lett. **72**, 3262 (1994).

[12] M.A. Continentino, Phys. Rev. B**47**, 11581; A.J. Millis, Phys. Rev. B**48**, 7183 (1993); A.M. Tsvelik and M. Reizer, Phys. Rev. B**48**, 9887 (1993).

[13] a) P. Nozières, P. and A. Blandin, J. Phys. (Paris) **41**, 193 (1980); b) D.L. Cox, Phys. Rev. Lett. **59**, 1240 (1987); c) Physica B **186-188**, 312 (1993).

[14] V. Dobrosavljević, T.R. Kirkpatrick, and G. Kotliar, Phys. Rev. Lett. **69**, 1113 (1992).

[15] O.O. Bernal *et al.*, Phys. Rev. Lett. **75**, 2023 (1995).

[16] B. Andraka and A. M. Tsvelik, Phys. Rev. Lett. **67**, 2886 (1991).

[17] W. Metzner and D Vollhardt, Phys. Rev. Lett. **62**, 324 (1989).

[18] E. Müller-Hartmann, Z. Phys. B **74**, 507 (1989).

[19] J. E. Hirsch, R. M. Fye, Phys. Rev. Lett.**56**, 2521 (1986); R.M. Fye and J.E. Hirsch, Phys. Rev. B **38**, 433 (1988).

[20] E. Miranda, V. Dobrosavljević and G. Kotliar, Phys. Rev. Lett. **78**, 290 (1997).

[21] R.N. Silver *et al.*, Phys. Rev. Lett. **65**, 496 (1990)

[22] For a review of the Maximum Entropy method of analytic continuation, see M. Jarrell, J.E. Gubernatis, Physics Reports Vol. **269** #3, (May, 1996).

[23] C. E. Shannon, Bell Syst. Tech. J. **27**, 379 (1948).

[24] Q.Si, J.Phys. :Cond. Matter **8**, 9953(1996) and references therein.

[25] S. Doniach and M. Sunjic, J.Phys.C **3**, 285 (1970).

[26] H.O. Frota and L.N. Oliveira, Phys. Rev. B **33**, 7871 (1986).

[27] P. Noziéres, J. Low Temp. Phys. **17**, 31 (1974).

[28] Th. Pruschke, M. Jarrell and J.K. Freericks, Advances in Physics **44**, 187-210 (March/April 1995).

[29] M. Jarrell, Hanbin Pang, D.L. Cox, F. Anders and Amit Chattopadhyay, unpublished (1996); F. Anders, and M. Jarrell, unpublished.

[30] Strictly speaking, since $P_{wd}(T_K)$ has a weak divergence like $1/(T_K ln^2 T_K)$ as $T_K \to 0$, the corresponding $\text{Im}\Sigma(\omega)$ also will contain a term like ω^α with $\alpha < 1$. However, the prefactor of this term is proportional to the relative weight of this singularity, which for our choice of parameters is about 10^{-7}. Hence, the term with the fractional power gets suppressed by the quadratic term for all experimentally accessible temperatures and frequencies.

[31] A. Chattopadhyay and M. Jarrell, Phys. Rev. B**56**, R2920 (1997).

[32] N. Andrei *et al.*, Rev. Mod. Phys. **55**, 331 (1983).

[33] See for example Fig. 25 and the discussion below in H.R. Ott, Progress in Low Temperature Physics, Vol. XI, ed. D.F. Brewer (Elsevier, Amsterdam, 1987), p. 216.

[34] F. Steglich, *et al.*, to be published in Physica B (1996).

[35] P.W. Anderson and Y. Ren, p. 3 of Ref. 1.

[36] M.A. Continentino, Phys. Rev. B**47**, 11581; A.J. Millis, Phys. Rev. B**48**, 7183 (1993); A.M. Tsvelik and M. Reizer, Phys. Rev. B**48**, 9887 (1993).

[37] a) P. Nozières, P. and A. Blandin, J. Phys. (Paris) **41**, 193 (1980); b) D.L. Cox, Phys. Rev. Lett. **59**, 1240 (1987); c) Physica B **186-188**, 312 (1993).

[38] Q. Si and G. Kotliar, Phys. Rev. Lett. **70**, 3143 (1993); Phys. Rev. B**48**, 13881 (1993); Q. Si, *et al.*, Phys. Rev. Lett. **72**, 2761 (1994).

[39] U. Brandt and C. Mielsch, Z. Phys. B **75**, 365, (1989); Z. Phys. B **79**, 295 (1990); Z. Phys. B **82**, 37 (1991); V. Janiš, Z. Phys. **B83**, 227(1991); C. Kim, Y. Kuramoto and T. Kasuya, J. Phys. Soc. Japan **59**, 2414(1990).; V. Janiš and D. Vollhardt, Int. J. Mod. Phys. **B6**, 713(1992); M. Jarrell, Phys. Rev. Lett. **69**, 168(1992); A. Georges and G. Kotliar, Phys. Rev. **B45**, 6479 (1992).

[40] Th. Pruschke, M. Jarrell and J.K. Freericks, Adv. in Phys. **42**, 187 (1995), and A. Georges, G. Kotliar, W. Krauth, and M. Rozenberg, Rev. Mod. Phys. **68**, 13 (Jan. 1996).

[41] K.-H. Luk, Mark Jarrell, and D.L. Cox, Phys. Rev. B, **50**,15864 (1994).

[42] M. Jarrell, H.-B. Pang, D.L. Cox, and K.-H. Luk, Phys. Rev. Lett. **77**, 1612 (1996).

[43] C.M. Varma, P.B. Littlewood, S. Schmitt-Rink, E. Abrahams and A.E. Ruckenstein, Phys. Rev. Lett. **63**, 1996(1989).

[44] D.L. Cox, to be published in Physica B (1996).

[45] D.J. Scalapino, S. White and S. Zhang, Phys. Rev. B, **47**, 7995 (1993).

[46] D.L. Cox and N. Grewe, Z. Phys. B**71**, 321 (1988).

[47] M. C. Aronson, J.D. Thompson, J. L. Smith, Z. Fisk, and M.W. McElfresh, Phys. Rev. Lett. **63**, 2311 (1989).

[48] F. Steglich, private communication (1996).

[49] D.A. Bonn et al., Physica C153-155, 453 (1988).

[50] T.M. Rice and K. Ueda, Phys. Rev. B**34**, 6420 (1988).

[51] N. Grewe, Th. Pruschke, and H. Keiter, Z. Phys. B**71**, 75 (1988).

[52] M. Jarrell, Phys. Rev. B**51**, 7429 (1995).